Modeling methane fluxes in wetlands with gas-transporting plants
3. Plot scale

Reinoud Segers and Peter A. Leffelaar

Group Plant Production Systems, Laboratory of Theoretical Production Ecology, Wageningen University, Wageningen, Netherlands

Abstract. A process model based on kinetic principles was developed for methane fluxes from wetlands with gas-transporting plants and a fluctuating water table. Water dynamics are modeled with the 1-D Richards equation. For temperature a standard diffusion equation is used. The depth-dependent dynamics of methane, oxygen, molecular nitrogen, carbon dioxide, soil carbon, electron acceptors in oxidized and in reduced form are affected by transport processes and kinetic processes. Modeled transport processes are convection and diffusion in the soil matrix, ebullition, and plant-mediated gas transport. Modeled kinetic processes are carbon mineralization, aerobic respiration, methane production, methane oxidation, electron acceptor reduction, and electron acceptor reoxidation. Concentration gradients around gas-transporting roots in water-saturated soil are accounted for by the models from the two previous papers, ensuring an explicit connection between process knowledge at the kinetic level (millimeter scale) and methane fluxes at the plot scale. We applied the model to a fen, and without any fitting, simulated methane fluxes are within 1 order of magnitude of measured methane fluxes. The seasonal variations however, are much weaker in the simulations compared to the measurements. Simulated methane fluxes are sensitive to several uncertain parameters such as the distribution over depth of carbon mineralization, the total pool size of reduced and oxidized electron acceptors, and the root-shoot ratio. Because of the process-based character of the model it is probable that these sensitivities are present in reality as well, which explains why the measured variability is usually very high. Interestingly, heterogeneities within a rooted soil layer seem to be less important than heterogeneities between different soil layers. This is due to the strong influence of the interaction between water table and profile scale processes on the oxygen input to the system and hence on net methane production. Other existing process models are discussed and compared with the presented model.

1. Introduction

High methane fluxes are often measured from wetlands with aerenchymateous plants that transport gases, such as rice paddies or sedge-dominated fens [*Prather et al.*, 1995, *Nykänen et al.*, 1998; *Bellisario et al.*, 1999]. Gas-transporting plants can affect methane fluxes both positively, by an escape route of methane to the atmosphere and by carbon substrates via root turnover or root exudation, or negatively, by allowing oxygen penetration into the soil [*Conrad*, 1993; *Wang et al.*, 1996]. Given these complex interactions, it is not surprising that there is a large unexplained variation in methane fluxes [*Moore and Roulet*, 1993; *Bartlett and Harris*, 1993; *Nykänen et al.*, 1998; *Bellisario et al.*, 1999] and the underlying processes [*Segers*, 1998]. Therefore a more fundamental understanding of methane fluxes is desirable using knowledge that is generally applicable: the theories of microbial and chemical conversions and physical transport processes. The scale at which this knowledge applies is called the kinetic scale, with a typical size of a few millimeters [*Segers and Leffelaar*, this issue].

This paper is the last paper in a series of three which aim to explicitly connect the knowledge at the kinetic level to methane fluxes at the plot scale. Mathematical modeling is used, because this is the most efficient way to integrate knowledge of several interacting processes across various spatial and temporal scales. In paper 1 [*Segers and Leffelaar*, this issue] the overall approach is discussed and a reaction-diffusion model was developed for processes around a single gas-transporting root. This model was successfully simplified by assuming a quasi-steady-state for oxygen and by spatially averaging the other compounds. In paper 2 [*Segers et al.*, this issue], methane dynamics are simulated in a water-saturated soil layer with gas-transporting roots. Here root architecture is described by a weight function for half the distance to the next root [*Rappoldt*, 1990,1992]. Spatially averaging at this scale had a small effect on net methane emission but a substantial effect on net methane production and methane transport.

In paper 3. we scale up to the plot scale. At this scale methane fluxes are not only determined by gas-transporting roots, but also by temperature and water table [*Moore and Roulet*, 1993; *Bartlett and Harris*, 1993; *Nykänen et al.*, 1998; *Bellisario et al.*, 1999]. Therefore the model is extended with modules for vertical transport of heat, water, and compounds. Furthermore, depth is introduced as an independent variable, as water content, temperature, root density, and decomposable organic matter vary with depth. As a result of

quasi-steady-state assumptions for some processes with characteristic times of a few hours [*Segers and Leffelaar*, this issue], the smallest timescale of interpretation is 1 day.

We focus on understanding the relations between the various scales and the relevance of smaller scales for understanding methane fluxes. Therefore we kept some processes and factors with a lot of uncertainties (such as temperature effects and seasonal dynamics of roots with respect to growth, decay, gas transport capacity, and exudation) as simple as possible, though these processes and factors may also be crucial in understanding methane fluxes. Consequently, in the analysis of model results we pay more attention to model behavior as such than to the comparison with measurements.

First, we describe the model and summarize information from literature, which is used for parameterization. Subsequently, we compare simulated methane fluxes with measured methane fluxes from an intensively monitored fen in the Netherlands [*van den Pol-van Dasselaar et al.*, 1999a, 1999b]. Effects of uncertainty in the parameters on simulated emissions are investigated by a sensitivity analysis. In addition, we tested the effects of model structure at the soil layer level [*Segers et al.*, this issue] on methane fluxes. Finally, we discuss the difference between our model and other process models for methane fluxes.

2. Model Description and Non-Site-Specific Parameterization

The core of the model is a set of coupled partial differential equations for water, heat, and species (CH_4, O_2, N_2, CO_2, labile soil carbon (c_{lab}), stable soil carbon (c_{stb}), and electron acceptors in oxidized form (eo) and reduced form (er) with time and depth as independent variables. The notation section lists the symbols.

2.1 Water

Water plays a crucial role in the aeration of the soil. As a first approximation, one might assume that above the water table the soil is aerobic, and below the water table the soil is anaerobic. However, reality is often more complicated. Firstly, the border between the oxic and the anoxic soil may be somewhat above the water table, especially in dense soil (deeper peat layers with higher water retention) (Tables 1 and 2). Secondly, upward and downward flow of water may affect methane fluxes by aqueous convective transport of methane and electron acceptors [*Romanowicz et al.*, 1993; *Waddington and Roulet*, 1997]. Thirdly, understanding of the

Table 1. Water Content θ (m³ H_2O m⁻³ soil) as a function of Water Potential pF and Dry Bulk Density ρ (kg m⁻³) for Peat Soils [*Paivanen*, 1973; *Okruszko and Szymanowksi*, 1992; *Loxham and Burghardt*, 1986; *Silins and Rothwell*, 1998]

pF	ρ <50	50 – 100	100 – 150	150 – 250
0	0 96 (0 03)	0.92 (0.04)	0 91 (0 02)	0 88 (0 03)
1	0.46 (0 29)	0 74 (0.20)	0 79 (0.11)	0 82 (0 04)
2	0 21 (0.12)	0.40 (0 15)	0 69 (0 08)	0.67 (0.06)
3	0 13 (0 08)	0.24 (0 07)	0 31 (0.10)	0.39 (0 05)

Standard deviations are within parentheses

Table 2. Coefficients c_1 and c_2 for Regression Equations of the Logarithm of Saturated Hydraulic Conductivity k_s in Relation to Bulk Density ρ in Peat ($^{10}log(k_s/k_{s,r}) = c_1 + c_2 \rho$).

c_1 (-)	c_2 (m³ kg⁻¹)	n	r^2	Source
-3.6	-0.016	<119	0 54	*Boelter* [1969]
-4 2	-0 0098	1280	0 22	*Paivanen* [1973]
-2.0	-0 027	80	0 73	*Silins and Rothwell* [1998]

Value $k_{s,r}$ is the reference value of k_s which is 1 m s⁻¹

episodic emissions of stored methane after a drop of the water table [*Windsor et al.*, 1992; *Shurpali et al.*, 1993] may require accurate information on the dynamics of gas-filled pore space to calculate the balance between methane release and methane oxidation regulated by oxygen inflow. To investigate these phenomena, a model is needed which simulates depth-dependent water content and bidirectional flow, driven by evapotranspiration and external hydrological conditions. Therefore we used the one-dimensional Richards equation [*Richards*, 1931, *Hillel*, 1971, p 109], which is an extension of Darcy's law with a relation between unsaturated hydraulic conductivity and water content.

To use the Richards equation, soil k-h-θ relationships are needed. These vary strongly for peat (Tables 1 and 2). Surface soil tends to be highly porous, with low bulk density, low water retention, and high hydraulic conductivity, whereas deeper soil and anthropogenically drained peat soil tends to have a higher bulk density, high water retention, and low hydraulic conductivity [e.g., *Silins and Rothwell*, 1998]. As first approach to catch the variation in hydraulic properties, the k-h-θ relationships were related to bulk density (Table 1, average of k from relations from Table 2 and Figure 1).

As a result of the decreasing hydraulic conductivity with depth, θ may get larger than θ_s when simulating an infiltration event, which is the result of considering only gravity and capillary forces. We coped with these problems by (1) starting rate calculations from the discretized soil layer with the water table, subsequently going upward and by (2) limiting downward flows with the downward flow to the next deeper layer (Appendix A).
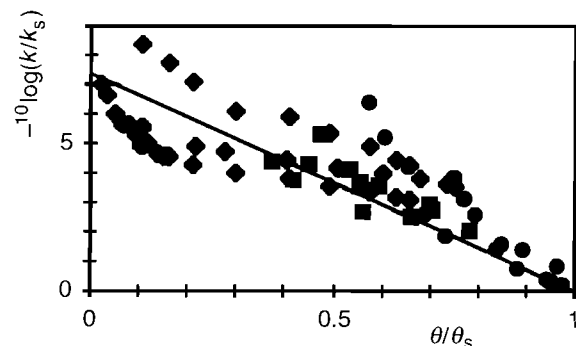

Figure 1. Relative unsaturated hydraulic conductivity (k/k_s) as function of normalized water content (θ/θ_s) for peat soils which were not or only moderately drained. Diamonds are from *Silins and Rothwell* [1998], dots are from *Schouwenaars and Vink* [1992], and squares are from *Loxham and Burghardt* [1986]. The line is a linear regression forced though (1, 0): $-^{10}log(k/k_s) = 7.4$ (1-θ/θ_s). r^2=0.56.

To apply the one-dimensional Richards equation, not only hydrological properties are needed but also expressions for water exchange between the soil column and the atmosphere and the deeper soil. Potential evapotranspiration (PET) is calculated from daily global radiation and daily air temperature using Makkink [1957]. PET is partitioned between potential evaporation and potential transpiration similar to light interception by plants [Belmans et al., 1983] with a roughly estimated leaf area index of 1 and an extinction coefficient of 0.7. Evaporation is the minimum of potential evaporation and the calculated water flux resulting from the pressure gradient between the first soil layer and the atmosphere [Feddes et al., 1988]. In our case, pressure heads are always above −1 m, so transpiration is always equal to potential transpiration [Feddes et al., 1978]. Transpiration is divided over the soil profile as a sink term in the water equation, weighed with root density. Ponding is allowed until a threshold, pond$_{thr}$. Ponded water above pond$_{thr}$ is assumed to run off with a time constant of 1 hour. Interception of precipitation is estimated using an empirical relation for grass [de Jong and Kabat, 1990]. The boundary condition at the water table is discussed in the model application section. Water fluxes below the water table are calculated in such a way that water contents below the water table remain saturated (Appendix A).

2.2 Temperature

As a simplest process-based approach, soil temperature could be modeled with a diffusion equation for temperature [e.g., Koorevaar et al., 1983]:

$$\frac{\partial T}{\partial t} = \frac{\partial}{\partial z}(\frac{\lambda_h}{c_p}\frac{\partial T}{\partial z}). \tag{1}$$

in which the heat conductivity λ_h and volumetric heat capacity c_p are related to the volumetric soil composition [Frolking and Crill, 1994]. The lower boundary is set at such a depth (4 m) that a zero gradient in temperature can be assumed (preliminary simulations and Puranen et al. [1999]). At the surface it is most simple to assume that soil temperature is equal to air temperature from weather data.

This simple approach is tested by considering more refined formulations for several parts of this model. The first refinement is to include the geometric arrangement of the soil components on λ_h [de Vries, 1963; ten Berge, 1990, p. 26]. The second is to include the effect of radiation on surface temperature (see section 3 3). The third is to include convection of heat, which may play a role in fens [van Wirdum, 1991]. This last process is modeled by using enthalpy h (J m^{-3} soil) as state variable, instead of temperature, keeping open the possibilities to extend the model with phase transitions (e.g., freezing), staying as close as possible to the underlying physics:

$$\frac{\partial h}{\partial t} = \frac{\partial}{\partial z}(\lambda_h\frac{\partial T(h)}{\partial z}) + \frac{\partial(v_wh)}{\partial z} + s_w\,h_w. \tag{2a}$$

$$T(h) = \frac{h}{c_p}. \tag{2b}$$

2.3. Species Dynamics

The species CH$_4$, O$_2$, CO$_2$, N$_2$, electron acceptors in reduced form and oxidized form and two soil carbon pools are modeled as a function of time and depth. In soil layers in which gas transport is dominated by gas-transporting plants the

gradients around gas-transporting roots are also considered, using models of the previous papers [Segers and Leffelaar, this issue; Segers et al., this issue].

2.3.1. Soil carbon and roots. To obtain a rough explanatory model for the depth distribution of soil carbon mineralization, three plant-related sources of soil carbon are distinguished. Firstly, the labile fraction of decayed roots; secondly, the labile fraction of decayed shoots; and thirdly, the stable fractions of decayed roots and shoots. The labile fractions are allocated into a labile soil carbon pool c_{clab} (z) and the stable fractions to a stable soil carbon pool c_{csb} (z). The labile soil carbon is spatially distributed close to the origin of the organic material: close to the surface for shoot litter (first term at right-hand side of equation (3a)) and proportional to root density for root litter (second term at right hand side of equation (3a) and right-hand side of equation (3b)):

$$\frac{\partial c_{clab}}{\partial t}|_{source} = \frac{f_C}{M_C}(\frac{f_{lab.sh}}{z_{littr}}\frac{C_{sh}}{\tau_{sh}} + f_{lab.rt}\frac{c_{rt}}{\tau_{rt}})\quad z<z_{littr} \tag{3a}$$

$$\frac{\partial c_{clab}}{\partial t}|_{source} = \frac{f_C}{M_C}f_{lab.rt}\frac{c_{rt}}{\tau_{rt}}\quad z>z_{littr} \tag{3b}$$

The stable soil carbon is distributed over the soil profile according to a fixed depth distribution $f_{stb}(z)$:

$$\frac{\partial c_{csb}}{\partial t}|_{source}$$

$$= f_{stb}(z)\frac{f_C}{M_C}((1-f_{lab.sh})\frac{C_{sh}}{\tau_{sh}} + (1-f_{lab.rt})\int_0^\infty\frac{c_{rt}(z)}{\tau_{rt}}dz). \tag{4}$$

The sink of each carbon pool is proportional to total C-mineralization ($s_{aecm}+s_{acm}$) and to the contribution of the pool to reference C-mineralization:

$$\frac{\partial c_{csb}}{\partial t}|_{source}\frac{\partial c_{clab}}{\partial t}|_{sink} = \frac{\frac{c_{clab}}{\tau_{clab}}}{\frac{c_{csb}}{\tau_{csb}}+\frac{c_{clab}}{\tau_{clab}}}(s_{aecm}+s_{acm}). \tag{5}$$

$$\frac{\partial c_{csb}}{\partial t}|_{sink} = \frac{\frac{c_{csb}}{\tau_{csb}}}{\frac{c_{csb}}{\tau_{csb}}+\frac{c_{clab}}{\tau_{clab}}}(s_{aecm}+s_{acm}). \tag{6}$$

Reference C-mineralization, which is the driver of aerobic and anaerobic C-mineralization as calculated according to Segers and Leffelaar [this issue], is related to the two carbon pools by

$$s_{rcm} = \frac{c_{csb}}{\tau_{csb}} + \frac{c_{clab}}{\tau_{clab}}. \tag{7}$$

To investigate the factors determining the relation between methane fluxes and easily measurable (aboveground) data, we consider aboveground biomass as site-specific data (Table 3) and we deduced the other plant and soil carbon parameters from the literature (Table 4). Two functional plant classes are distinguished: mosses without roots and non-mosses with gas-transporting roots. Nonmosses without gas-transporting are not explicitly considered but could be seen as nonmosses with low gas transport capacity. Both types of plants act as a source for the soil carbon model (equations (3)-(4)), only the nonmosses contribute to root gas transport. The allocation of carbon over depth to the stable carbon pool, $f_{stb}(z)$, is taken as an exponential function with a characteristic depth, $d_{chr.cs}$.

Table 3. Properties of Koole, Brampjesgat (Bramp), and Drie Berken Zudde (DBZ).

Property	Koole	Bramp	DBZ	Note
Measured				
harvested shoots nonmosses, kg dw m^{-2}	0.16 (0.07)	0.35 (0.23)	0.16 (0 04)	a b
harvested mosses, kg dw m^{-2}	0.21 (0.08)	0.12 (0.09)	0.29 (0 03)	a b
bulk density, kg dw m^{-3}, (0–5 cm)	120 (100)	76 (20)	77 (20)	a
(5–10 cm)	140 (110)	152 (50)	149 (90)	a
(10–20 cm)	200 (100)	237 (40)	190 (70)	a
average groundwater level, m	0.09	0 11	0.18	c
Deduced/assumed				
$f_{ms\ hat}$	0.25	0 25	0 5	d
shoots of nonmosses, kg dw m^{-2}	0.21	0 47	0.21	e
mosses, kg dw m^{-2}	0 84	0 48	0 58	e
$d_{chr\ rt}$, m	0 1	0 1	0.2	f
dtlevl, m	0.12	0 14	0.22	g
R_{ditch}, 10^6 s	7	3	4	g

The standard deviation (n=6) is in parentheses. ND means not determined.

aA. van den Pol-van Dasselaar (Wageningen University, unpublished data, 1998)

b1994-1996 for Koole and Bramp, 1994,1996 for DBZ.

cvan den Pol-van Dasselaar et al., [1999a]

dEstimated.

eCalculated with equation (17).

fAt DBZ roots were assumed to be deeper in the profile due to the deeper water tables, which was confirmed by root measurements (A van den Pol-van Dasselaar, Wageingen University, unpublished data, 1998).

gFitted.

Turnover of soil carbon and vegetation are assumed to depend on temperature with a Q_{10} of 2 and with reference temperature at average air temperature. Generally, roots do not penetrate deeply in freshwater wetlands, though quite some variation is present (Figure 2). Little is known about the causes of this variation. *Miller et al.* [1982] suggested that root depth in peats is controlled by nutrient availability. *Metsävainio* [1931] found a much higher percentage of dead roots below the water table than above, indicating that despite the adaption mechanisms, roots of wetland plants are hampered under anoxic conditions. As default, we assumed that root density c_{rt} decreases exponentially with a characteristic depth, $d_{chr.rt}$ of 0.1 m:

$$c_{rt} = \frac{C_{it}}{d_{chr.it}} \exp\left(-\frac{z}{d_{chr.rt}}\right) \tag{8}$$

2.3.2. Homogeneous concentrations in water-unsaturated soil and heterogeneous concentrations in water-saturated soil.

In water-saturated soil, gas exchange between soil and atmosphere is controlled by transport via the roots and aqueous diffusion around the roots. This diffusion process is slower than several reactions, resulting in heterogeneous concentrations of several species at a certain depth [*Segers and Leffelaar*, this issue]. In the oxic, water-unsaturated soil, gas exchange is controlled by transport via the gaseous pores and diffusion through water films around soil particles. In nonaggregated or dry soils these water films will be thin, resulting in fast diffusion processes in the films and in homogeneous species concentrations at each depth. In aggregated moist soil the aqueous volumes may be so large that diffusion is slower than reaction, resulting in heterogeneous species concentrations (e.g., partial anaerobiosis). However, in the top soil of undrained peat, water retention is low, and no clear aggregation is present. Therefore as first approach, it is

assumed that in the water-unsaturated surface soil the concentrations are homogeneous at each depth. As a result of the different behavior in the two zones of the soil, we applied different models for each zone (Figure 3).

The functional difference between the homogeneous and the heterogeneous zone, as defined above, is reflected in the oxygen behavior. In the water-unsaturated zone, oxygen is amply available and supplied by vertical transport via the soil matrix, and in the water-saturated zone, it is scarce and supplied by gas-transporting plants. Therefore the occurrence of the heterogeneous regime is not directly governed by the water table but by three conditions, related to gas transport and aeration:

$$\overline{c}_{aq.O_2} < 0.1 \, f_{hyst}\, \alpha\, \overline{c}_{g.O_2.atm}, \tag{9a}$$

$$\overline{q}_{O_2} > f_{hyst}\, \overline{sj}_{O_2}. \tag{9b}$$

$$k > k_c. \tag{9c}$$

The first condition (9a) prescribes that the oxygen concentration should be low; f_{hyst} is a factor (0.95 in unsaturated conditions and 1.05 in saturated conditions) to prevent oscillations in model structure. The second condition (9b) prescribes that plant-mediated oxygen transport, $\overline{q}_{O_2}$, should be faster than matrix oxygen transport. The third condition (9c) is included for technical reasons. It prescribes that the soil can only be considered heterogeneous if the soil gas phase is discontinuous, as the state events associated with convective transport (occurring only in gas-continuous soil) are not implemented for heterogeneous soil.

2.3.3. Heterogeneous zone, gas exchange dominated by gas-transporting roots.

As a starting point, we take the full soil layer model of the previous paper [*Segers et al.*, this issue]. In this model a rooted soil layer is

Table 4. Default Nonsite-Specific Parameters.

Parameter	Value	Notes
$f_{sh,hat}$	0 75	a
z_{hu}, m	0 05 (0 05-10)	a
$d_{chi\ cs}$, m	0 2 (0 1-0.5)	b
RSR	1 (0 2-10)	c
$f_{lab,sh}$	0 5	d
$f_{lab,ms}$	0 2	c
τ_{sh}, s	3 2×10⁷	a
τ_{il}, s	6 3×10⁷	f
τ_{clab}, s	6 4×10⁷	g
τ_{csib}, s	3 2×10⁹	h
rhizosphere geometry	cylindrical (spherical)	i
k_{il}, m³ H₂O m⁻² soil s⁻¹	10⁻⁷ (10⁻⁶-10⁻⁷)	i
ψ_{il}", mol O₂ m⁻² active root s⁻¹	10⁻⁸ (10⁻⁸-5×10⁻⁸)	i
c_{eiot}, mol el eqv m⁻³ soil	50 (5-100)	i
Vm_mo, mol m⁻³ soil s⁻¹	10⁻⁵ (10⁻⁶-10⁻⁴)	k
kinetics	l	l
root architecture	m	m
bubble transport	l	l
$\varepsilon_{g\ cl}$, m³ gas m⁻³ soil	0 05	n
$D_{aq,ell}$	depends on θ	o

Investigated range in sensitivity analysis is within parentheses
a Estimated
b Fitted by eye (Figure 7)
c Brinson et al [1981], Shaver and Chapin [1991], Wallen [1986], Sjors [1991], Saarinen [1996], Bernard et al. [1988], R K Wieder, Villanova University, personal communication, 1999
d Typha, Phragmites, Scolochloa, Scirpus [Wrubleski et al, 1997]
e Johnson and Damman [1993]
f Carex rostrata [Saarinen, 1996]
g Szumigalski and Bayley [1996], Thormann and Bayley [1997], and Wrubleski et al. [1997].
h Taken much larger than the scale of experiments
i Combination of rhizosphere geometry k_{il} and root oxygen consumption ψ_{il}" leading to an intermediate root oxygen release and gas exchange between rhizosphere and atmosphere [Segers et al., this issue]
j Somewhat higher than in the work of Segers and Kengen [1998], because they only considered electron acceptors in oxidized form
k Average of wetlands [Segers, 1998] and few measurements at Koole [Heipieper and de Bont, 1997]
l Segers and Leffelaar [this issue]
m Segers et al. [this issue]
n Sandy loam [Leffelaar, 1988].
o Campbell [1985] and molecular diffusion coefficients similar to Segers and Leffelaar [this issue]

represented by a set of weighed single root model systems with different radii, R_m. The weights, w_m, are used to calculate the spatially averaged concentrations at the soil layer level, $\bar{c}$, from the concentrations at the single root level, $\bar{c}$:

$$\bar{c}_i(z,t) = \sum_{m=1}^{N'} w_m(z)\,\bar{c}_{i,m}(z,t) \tag{10}$$

The dynamics of each concentration c_i in each single-root model system m are calculated with the simplified single-root model [Segers and Leffelaar, this issue]. In this paper we introduce a vertical coordinate, resulting in vertical gradients, causing diffusion and mass flow which may affect processes on the single root scale. Timescales of these transport processes are generally larger than the timescales of the processes around the single root. Therefore the fast interactions, as described in the single-root paper [Segers and Leffelaar, this issue], will

not be affected and the tested simplifications will remain valid. Instead, the vertical transport processes may cause a slow change of concentrations of solutes and gases. To account for this effect, the vertically discretised rate equations for the concentrations at the single-root scale are extended with a vertical transport term, $s_{j,i,m,k}$:

$$\frac{\partial \bar{c}_{i,m,k}}{\partial t} = \bar{s}_{i,m,k} + \bar{q}_{i,m,k} + \bar{b}_{i,m,k} - \bar{b}_{i,k+1} + \bar{s}_{j,i,m,k}. \tag{11}$$

Expressions for kinetics $\bar{s}_i$, plant-mediated transport $\bar{q}_i$, and bubble release b_i, (by definition negative) are in the work of Segers and Leffelaar [this issue]; $\bar{b}_{i,k+1}$ is the bubble release from the next deeper discretized soil layer. The aqueous concentrations of the gases are calculated from the soil volume concentrations by assuming temperature-dependent equilibrium between the gas and the water phase using Wilhelm et al. [1977]. $s_{j,i,m,k}$ is discussed in section 2.3.5.

As an alternative for equations (10)-(11), models were deduced [Segers et al., this issue] in which the dynamics in N weighted single-root model systems are replaced by soil layer averaged equations. Incorporation of vertical transport in these models is straightforward:

$$\frac{\partial \bar{c}_{i,k}}{\partial t} = \bar{s}_{i,k} + \bar{q}_{i,k} + \bar{b}_{i,k} - \bar{b}_{i,k+1} + \bar{s}_{j,i,k}. \tag{12}$$

$\bar{s}_{j,i}$ is discussed in section 2.3.5. Segers et al. [this issue] discuss two methods to calculate $\bar{s}_i$, $\bar{q}_i$, and b_i from soil layer averaged concentrations $\bar{c}$: the simplified soil layer model and the homogeneous soil layer model.

In the simplified soil layer model a soil layer is split into two fractions: oxygen saturated and oxygen unsaturated. Methane concentrations and electron acceptor concentrations are modified according to the aeration status, and these modified concentrations are used to calculate kinetics and
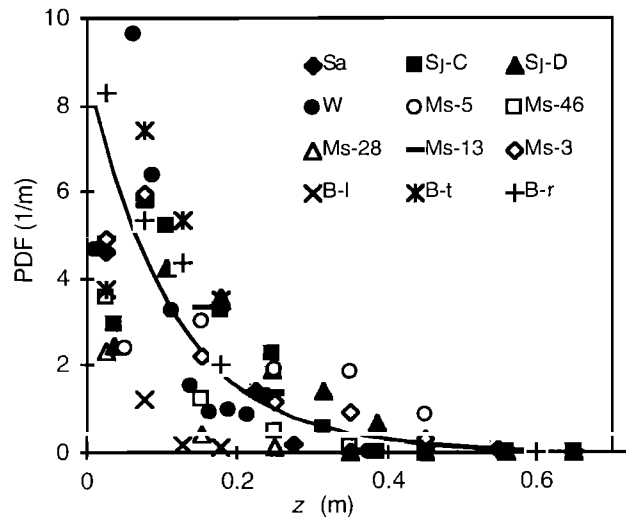

Figure 2. Probability density function, PDF, for root density (in kg dw m⁻³) related to depth z in freshwater wetlands. Sa: Saarinen [1996]; Sj: Sjors [1991] site C and D; Ms Metsävainio [1931] sites 3, 5, 13, 28, 46; W: Wallén [1986] and B Bernard and Fiala [1986] Carex lasiocarpa (l), C. rostrata (r), and C. trichocarpa (t). The solid line is the function $1/d_{chi\ it}\exp(-z/d_{chi\ it})$, where $d_{chi\ it}$ is the fitted ($r^2=0.54$) characteristic depth with value 0 11 m
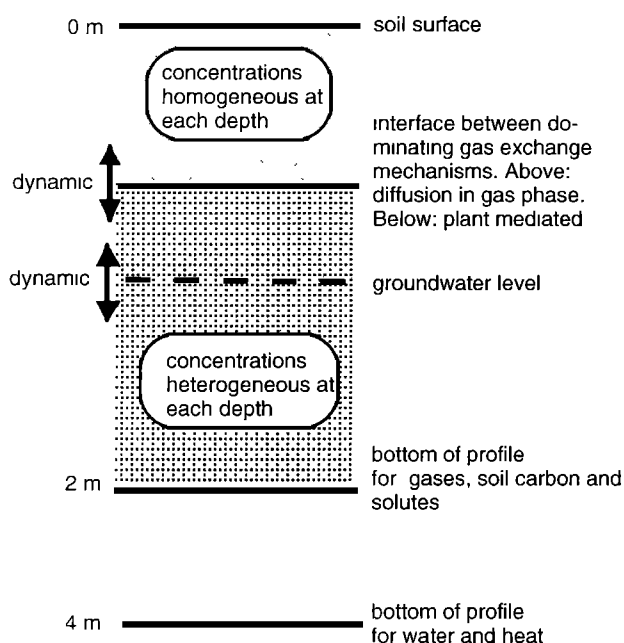
Figure 3. Overview of the model structure. For explanation and discussion see text.

transport in both fractions. Finally, weights of the fractions are used to calculate the soil layer averaged rates.

In the homogeneous soil layer model the soil layer averaged concentrations are directly used in the kinetic model [*Segers and Leffelaar*, this issue, equations (10)-(33)] and in the bubble model [*Segers and Leffelaar*, this issue, equations (4)-(8)], and plant-mediated gas transport is related to soil-layer averaged concentrations with an average first-order exchange coefficient [*Segers et al.*, this issue, equation (1), *Segers and Leffelaar*, this issue, equations (60)-(61)].

As default, we use the simplified soil layer model (equation (12)), as it was considerably faster than the full soil layer model (equations (10)-(11)), while preliminary simulations showed that model results were comparable (Figure 13, discussed later).

2.3.4. **Homogeneous zone, gas exchange dominated by diffusion in gaseous pores.** As argued above, we assume that in this zone the soil is homogeneous at each depth, which leads to the homogeneous soil layer model (see above and *Segers et al.* [this issue])

2.3.5. **Vertical mass transport by diffusion and aqueous convection.** Aqueous convection of gases and solutes is modeled with a standard equation, just as diffusion in both the gas and the aqueous phase (Ficks law):

$$\overline{sj}_{t,k} = -\frac{\partial(\nu_w \overline{c}_{aq,t})}{\partial z} \mathbf{l}_k + \frac{\partial}{\partial z} (D_{g,eff,t} \frac{\partial \overline{c}_{g,t}}{\partial z}) \mathbf{l}_k. \qquad (13)$$

Hydrodynamic dispersion is neglected for reasons of simplicity and because it is less important than convection. Various relations have been suggested to relate $D_{g,eff}$ to $D_{g,0}$, accounting for tortuosity and constructivity (Figure 4). The formulation of *Millington and Shearer* [1971] for nonstructured soils can be considered as a kind of lower limit for the diffusion reduction factor. The relation of *Campbell* [1985] may be used as best estimate, if no other information is present and proved to be reasonable for a drained peat soil [*Dunfield et al.*, 1995]. As default, we use the relation of

Campbell [1985] with temperature dependent $D_{g,0}$ from *Hirschfelder et al.* [1964] using *Leffelaar* [1987].

Because of the linearity of the transport equations and because of the scale difference between the discretised vertical dimension ($\approx$ a few centimeter) and the microdimension ($\approx$ a few millimeter) the influence of vertical transport on the dynamics in a single-root model system m ($sj_{m,t}$) can be described with

$$\overline{sj}_{m,t,k} = \overline{\overline{sj}}_{t,k} + \xi_{mix,sj,k} (\overline{c}_{t,k} - \overline{c}_{m,t,k}), \qquad (14)$$

where $\overline{\overline{sj}}_{t,k}$ is the ordinary, mean, vertical transport (equation (13)), and $\xi_{mix,sj,k}$ (s^{-1}) is an apparent mixing coefficient, which depends on the rates of vertical transport (Appendix B).

2.3.6. **Vertical mass flow by convection in the gas phase.** When the soil is gascontinuous ($\varepsilon_g > \varepsilon_{g,ci}$, [*Leffelaar*, 1988]), convection in the gas phase is an extremely fast process, driven by pressure gradients, caused by (1) release of stored gases after drying of the soil, (2) deficiencies of Fick's law, (3) unequal molar production and consumption of gases [*Leffelaar*, 1988], and (4) unequal gas solubilities in water. Time-explicit simulation of gas - continuous convection results in impractically small time steps. Therefore we modeled this process as a state event [*Leffelaar*, 1999], following *Leffelaar* [1988, equation (14)], occurring when the pressure difference between soil and atmosphere is larger than 0.1%.

2.4. Boundary Conditions and Initial Values

For water and temperature the lower boundary was set at 4 m (see section 2.2). For the other compounds it was set at 2 m. At this boundary the sum of the electron acceptors in reduced and oxidized status was the same as in the bulk of the soil with 95% in reduced status. Both at the bottom of the profile and at the soil surface the gases were in equilibrium with the atmosphere, except for c_{O_2} at the bottom, which was set to zero. Gas composition in precipitation was in equilibrium with the atmosphere, while electron acceptor concentrations were assumed to be zero.
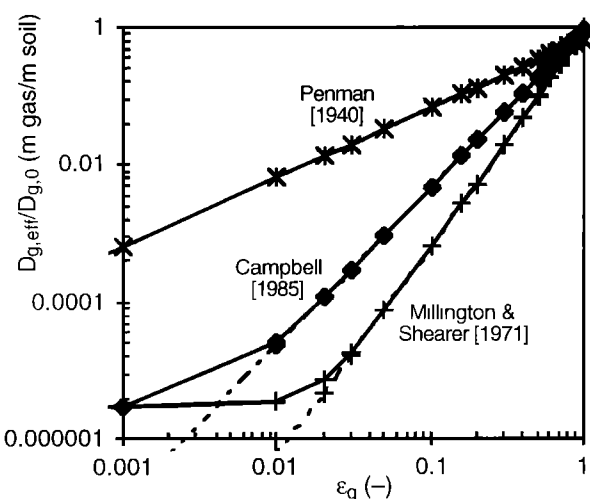

Figure 4. Overview of relations for relative diffusion coefficient. $D_{g,eff}/D_{g,0}$, as function of gas-filled pore space, ε_g. The dashed lines are the original relations from literature in which aqueous diffusion is neglected. The solid lines are the same relations, extended with an aqueous diffusion component similar to *Leffelaar* [1988].

To reduce the effect of initial conditions on results, simulations were always started in the spring about 0.75 year before interpretation of the data. This is sufficient for most processes, as they have characteristic times less than 1 year. Because soil carbon dynamics are much slower, we used equilibrium values of the soil carbon pools as initial conditions. These were analytically estimated with, depth-dependent, 3-year-averaged aeration from preliminary simulations.

2.5. Computational Considerations

Spatial discretization is according to the control volume method [*Patankar*, 1980], ensuring conservation of mass. For convection we used an upwind scheme. Differences with the more accurate hybrid upwind/central scheme [*Patankar*, 1980] were investigated and are small (data not shown). For the vertical discretization we used 15 soil layers (6 × 0.02, 0.03, 3 × 0.05, 2 × 0.1, 0.5, 1 and 2 m thick). A finer grid results in similar simulation results (average differences in flux < 1 %), apart from some peaks in methane fluxes which differ in magnitude (up to 300%) when plotted once a day. The problem is minimized by analyzing daily averaged methane fluxes, which are much less sensitive to the spatial discretization (differences in peaks of methane fluxes < 30 %) than the fluxes at a point in time.

For the temporal discretization we used the explicit Euler method with a dynamic time step. For each state at each time step, a maximum time step was estimated as a fraction of the inverse of the relative rate of change. This fraction was different for the water, heat, and gas state variables and set at the largest value which did not affect simulation results. Integration of all the states was performed with the smallest maximum time step. As the water model requires the smallest time steps but relatively few calculations per time step, this submodel was run separately and its output was used as input for the heat and gas model.

Mass balances for the gases, the electron acceptors, carbon, water, and heat were calculated to check the code. The Fortran code containing the integrated models of the three papers is available upon request.

3. Application of the Model at the Nieuwkoopse Plassen Area

3.1. Site Description

The Nieuwkoopse Plassen area is a nature preserve in the western part of the Netherlands. Mean monthly temperatures range between 2° and 17°C. Mean air temperature is 9 °C. Precipitation is about 800 mm and potential evapotranspiration is about 550 mm. The area consists of lakes, partly floating fens, and ditches. The vegetation, a mixture of grasses, sedges, rushes, mosses and reed, is mown and removed annually to preserve the vegetation. For the same reason the water level in the surface water is as much as possible maintained at a constant level (fluctuations are less than 5 cm). At three sites in the area, Koole, Brampjesgat, and Drie Berken Zudde, methane fluxes, soil temperature and water table were monitored approximately biweekly for almost 3 years [*van den Pol-van Dasselaar et al.*, 1999a]. Vegetation and soil were analyzed after the monitoring experiment [*van den Pol-van Dasselaar et al.*, 1999b]. Daily precipitation is taken from the experimental farm ROC Zegveld (less than 5 km
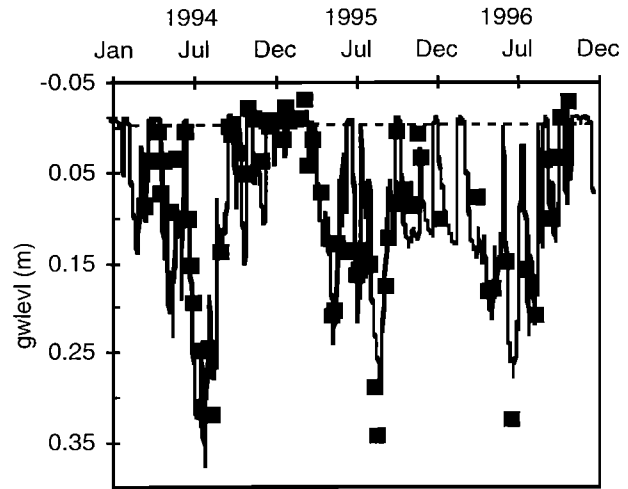

Figure 5. Simulated (line) and measured (squares) [*van den Pol-van Dasselaar et al.*, 1999a] groundwater level at the site Koole. Fitted parameters: dtlevl=0.12 m and $R_{ditch}=7×10^6$ s.

away). Daily total incoming and daily maximum and minimum temperatures are from de Bilt (about 25 km away).

Air pressure and water column height may influence bubble pressure and bubble release. However, we neglected these effects by putting bubble pressure at a constant value of 10^5 Pa, because there are no indications that ebullition is an important emission pathway at this site [*van den Pol-van Dasselaar et al.*, 1999a] and because of preliminary calculations.

3.2. Water

Groundwater level in fens is controlled by weather and site-specific hydrological conditions. Ditches strongly influence water movement at our site. This was incorporated in our model by a boundary condition at the bottom of the water-unsaturated zone [*van Bakel*, 1986]:

$$v_{w.gwlevl} = \frac{dtlevl - gwlevl}{R_{ditch}} \tag{15}$$

The nontrivial discretization of this boundary condition is described in Appendix A. Constant ditch level (dtlevl) and the constant resistance for water exchange between plot and ditch (R_{ditch}) were fitted by eye using biweekly measured groundwater levels (gwlevl) [*van den Pol-van Dasselaar et al.*, 1999a]. The area is flat, and therefore we assume that little water can be stored as ponded water (pond$_{thr}$ = 0.01 m).

From the literature we derived hydraulic properties as a function of bulk density (Tables 1 and 2). When using typical fen bulk densities also from literature [*Minkkinen and Laine*, 1996], it was not possible to obtain a reasonable fit for the simulated water table at our sites. However, when using the measured bulk densities (Table 3), it was possible (Figure 5, Table 3). This can be explained by the much lower bulk density for the typical fen (50-110 kg m^{-3}) compared to our site (100–200 kg m^{-3}) and the sensitivity of hydraulic properties for bulk density within the considered range.

3.3. Soil Temperature

Diurnal variation in air temperature is calculated with a sine function, using minimum and maximum temperatures from the weather data. Porosity and dynamic volumetric water content
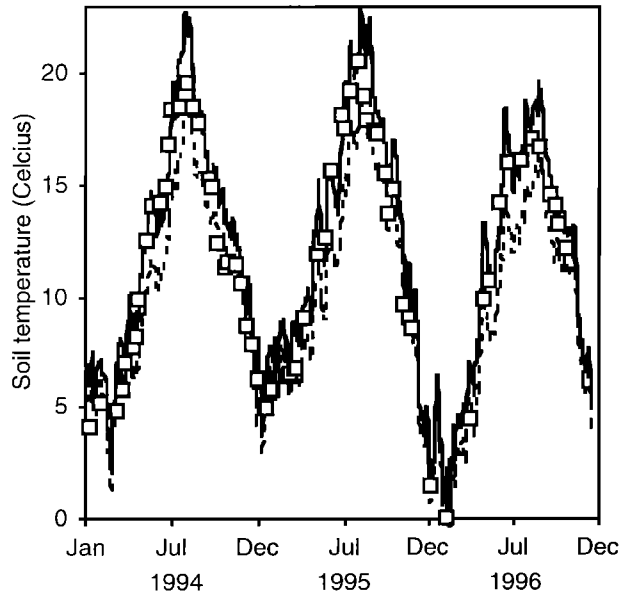
Figure 6. Simulated (lines) and measured (symbols) (A. van den Pol-van Dasselaar, Wageningen University, unpublished data, 1998) soil temperatures at 0.3 m depth at Koole. The dashed line is the result from the temperature diffusion equation (1) with surface temperature equal to air temperature. The drawn line is the result from the same model with a different boundary condition at the surface (equations (16)).

are taken from the water model. The solid phase is assumed to consist of 100% organic matter. In the model description, three options for refining the temperature model were discussed. We tested these options by taking the simplest model as default and by subsequently running the model with one added refinement each time.

Including convection and the way of calculating conductivity has very little effect on simulated soil temperatures (data not shown), just like changing the composition of the solid phase from 100% organic matter to actually measured values (80% organic matter and 20% clay [van den Pol-van Dasselaar et al.,1999a]) (data not shown). Apparently, the water phase dominates the heat transport. However, including radiation in the boundary condition at the surface (equations (16), a linear regression with measured surface temperatures in 1994 at the three sites (A. van den Pol-van Dasselaar, Wageningen University, unpublished data, 1998), did have an effect and improved simulated soil temperatures (Figure 6).

$$T_s = T_{air} + a_1 \text{ rad} + a_2,$$ (16a)

$$a_1 = 0.015 \text{ K m}^2 \text{ s J}^{-1},$$ (16b)

$$a_2 = -0.4 \text{ K}.$$ (16c)

Therefore in the remaining part of the paper we used the simplest soil temperature model (equation (1)) with boundary conditions (equation (16)).

3.4. Soil Carbon Dynamics

The soil carbon model (equations (3)-(8)) requires standing biomass as site-specific input. In 1994 and 1995 the vegetation was cut at about 5 cm above the soil surface in

summer, similar to the usual nature management at our site. In 1996 it was cut at the surface. Dry weights of the cut vegetation [van den Pol-van Dasselaar et al., 1999b] averaged over 1994-1996, and estimated harvested fraction were used to estimate standing biomass:

$$C_{sh} = \frac{C_{sh.har}}{f_{sh.har}}.$$ (17)

Furthermore, the input to the soil carbon pools from the shoots (equations (3a) and (4)) is reduced by a factor $(1-f_{sh.har})$. For the short mosses, $f_{sh.har}$ is estimated at 0.25, and for longer shoots, it is estimated at 0.75. To estimate the initial size of the carbon pools, time-averaged depth-dependent aeration (oxygen supply/oxygen demand) was used (see subsection on boundary conditions and initialization). Preliminary simulations showed that it varied roughly linearly with depth from 80 % at the surface to 0 % at 0.4 m. As default, $d_{chr.cs}$ was fitted by eye at 0.2 m using laboratory data on C-mineralization (Figure 7).

In medium-term (90 days) slurry incubations [S. W. M. Kengen, Wageningen University, unpublished data, 1996] (see Segers and Kengen [1998] for details on methods), an overestimation of C-mineralization may be expected due to the continuous shaking of incubation vessels and possibly due to the removal or dilution of toxic compounds [Williams and Crawford, 1984, Magnusson, 1993; Brown, 1998]. Figure 7 shows that C mineralization and its dependence on depth are sensitive for root-shoot ratio and the characteristic depth of the stable carbon pool. When roots are an important carbon source, as for example for simulations at Brampjesgat (data not shown), also characteristic root depth ($d_{chr\,rt}$) influences the depth profile of C-mineralization.
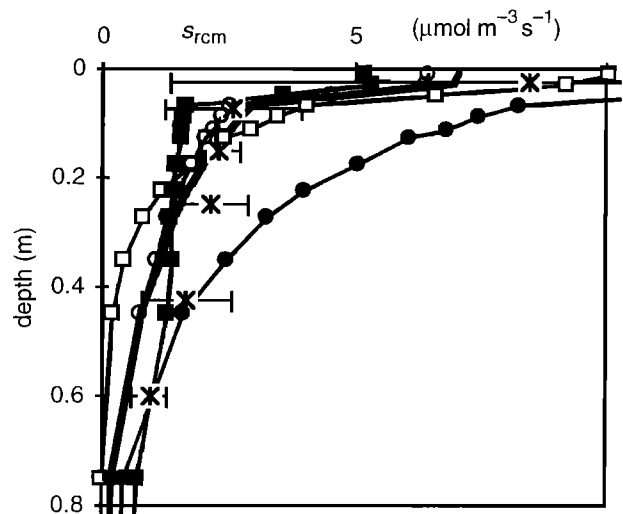

Figure 7. Reference C-mineralization at Koole as function of depth. Time-averaged (1994-1996). The asterisks are deduced from an incubation study (S. W. M Kengen, Wageningen University, unpublished data, 1996). The error bars represent 1 standard deviation (n=2). Note that the error bar of the most shallow measurement does not completely fit in the graph. The lines with dots are results from the simulation with default parameters, except for RSR, which was 10 (solid circles) and 0 2 (open circles). The lines with squares are results from the simulation with default parameters, except for $d_{chr\,cs}$, which was 0 5 m (solid squares) and 0.1 m (open squares). The thick line is the simulation with default parameters (Tables 3 and 4) (RSR=1 and $d_{chr.cs}$=0.2 m).

Several parameters ruling the soil carbon model are estimated and hence not accurate. By more accurate measurements some estimates (e.g., harvested fractions) could have been improved rather easily. However, it is doubtful whether this would improve the accuracy of the total soil carbon model, as several other parameters are hard to measure accurately (e.g. root turnover). The sensitivity of simulated methane emissions for various soil carbon parameters is investigated in section 3.5.
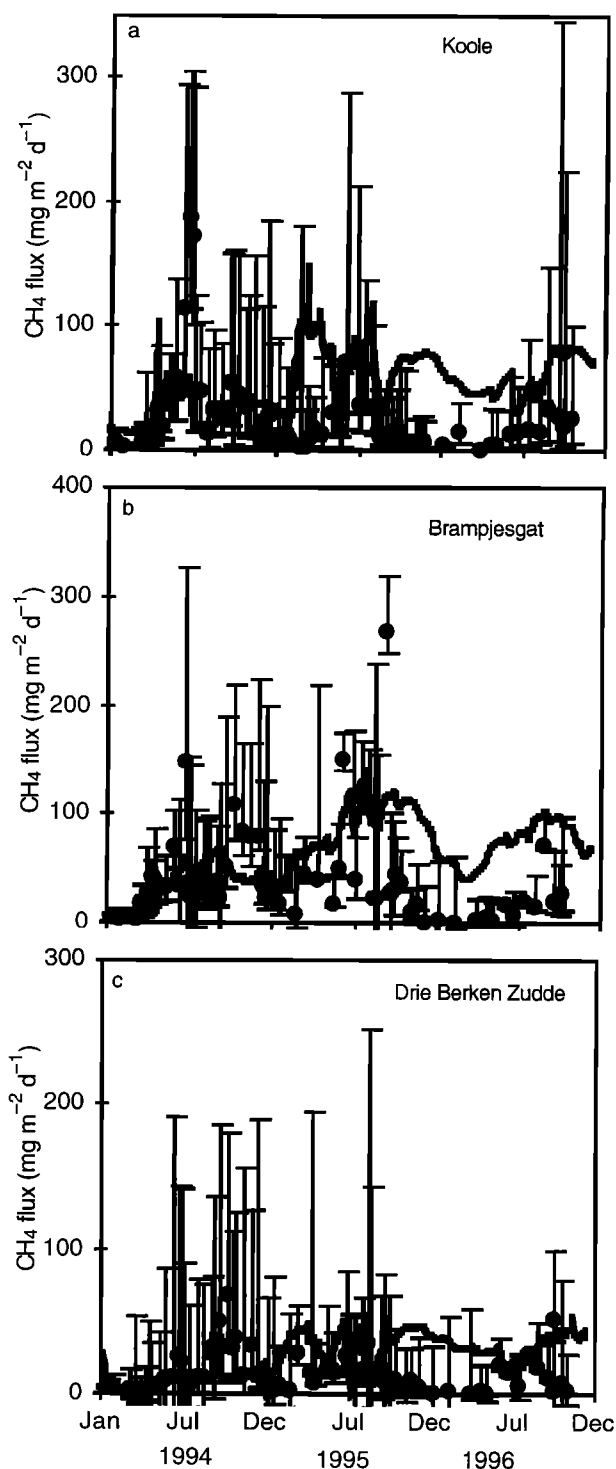
3.5 Methane Fluxes

Reasonable simulations seem possible for water, heat, and carbon dynamics, a prerequisite for process-based simulation of methane fluxes. A default parameterization for the methane kinetics and root parameters is obtained from literature data (Table 4) and easily measurable site-specific information (Table 3). This default parameterization is used as reference for a sensitivity analysis in which at least one parameter of each uncertain process was varied over a plausible range.

The order of magnitude of simulated methane fluxes with the default parameterization corresponded with the measured methane fluxes (Figures 8). Also, the model produces lowest methane emissions for Drie Berken Zudde, the site with the lowest measured emissions. However, the simulated seasonal variation is too small and sometimes even wrong. Especially simulated winter fluxes are too high. To investigate this discrepancy, we varied several uncertain parameters (Figures 9). From this analysis it is clear that fluxes may change more than an order of magnitude upon changes in parameters, which is in line with the large spatial variability of observed methane fluxes.

Furthermore, it is clear that none of the simulations captures the low winter fluxes (especially those in the relatively cold winter of 1995/1996, Figures 6 and 8). This may be due to the assumption that root gas transport capacity is static and is not reduced in winter. Another possible explanation is the absence of a fast soil carbon pool fed by a seasonal source (root exudates or decaying roots).

Also, methanogenic bacteria may be hampered at low temperatures resulting in a limitation of methane production by methanogenic activity [Shannon and White, 1996; Drake et al., 1996], which is not included in our model. Introducing a separate temperature sensitivity for methane production implies the possibility that methane production is limited by the activity of methanogenic bacteria. This would mean that (temporarily) accumulation of methanogenic substrates would have to be included, which means an extra state variable at all spatial scales and additional uncertain sensitive parameters. Before doing so, it seems wise to collect more direct experimental evidence for the extreme temperature sensitivity of methanogenic bacteria, as the strong temperature response of methane emissions from soil samples may also be the result of the interaction between processes with modest temperature sensitivity [van Hulzen et al., 1999]. At low temperatures also the Q_{10} of C-mineralization is often higher than 2 [Chapman and Thurlow, 1998]. However, it is not likely that this explains the too high winter fluxes, because simulated methane fluxes are already too high in autumn when soil temperatures are still about 10°C.

In 1996, measured methane fluxes were lower than in other years, possibly because of lower water tables [van den Pol-van Dasselaar et al., 1999b]. However, the simulations do not reproduce this interannual trend, probably because the

Figures 8. (a-c) Simulated daily averaged methane fluxes (lines) and measured methane fluxes (circles) [van den Pol-van Dasselaar et al., 1999a]. The error bars indicate 1 standard deviation of the log-transformed methane fluxes (n=6). Note the differences in y axis.

model is not sensitive enough for water table. This may be due to a too large role of deeper soil layers, caused by too many roots at greater depth and/or too high carbon availability at greater depth.

It would be possible to find a better fit for these sites by adapting (several) model parameters and/or model structure, but
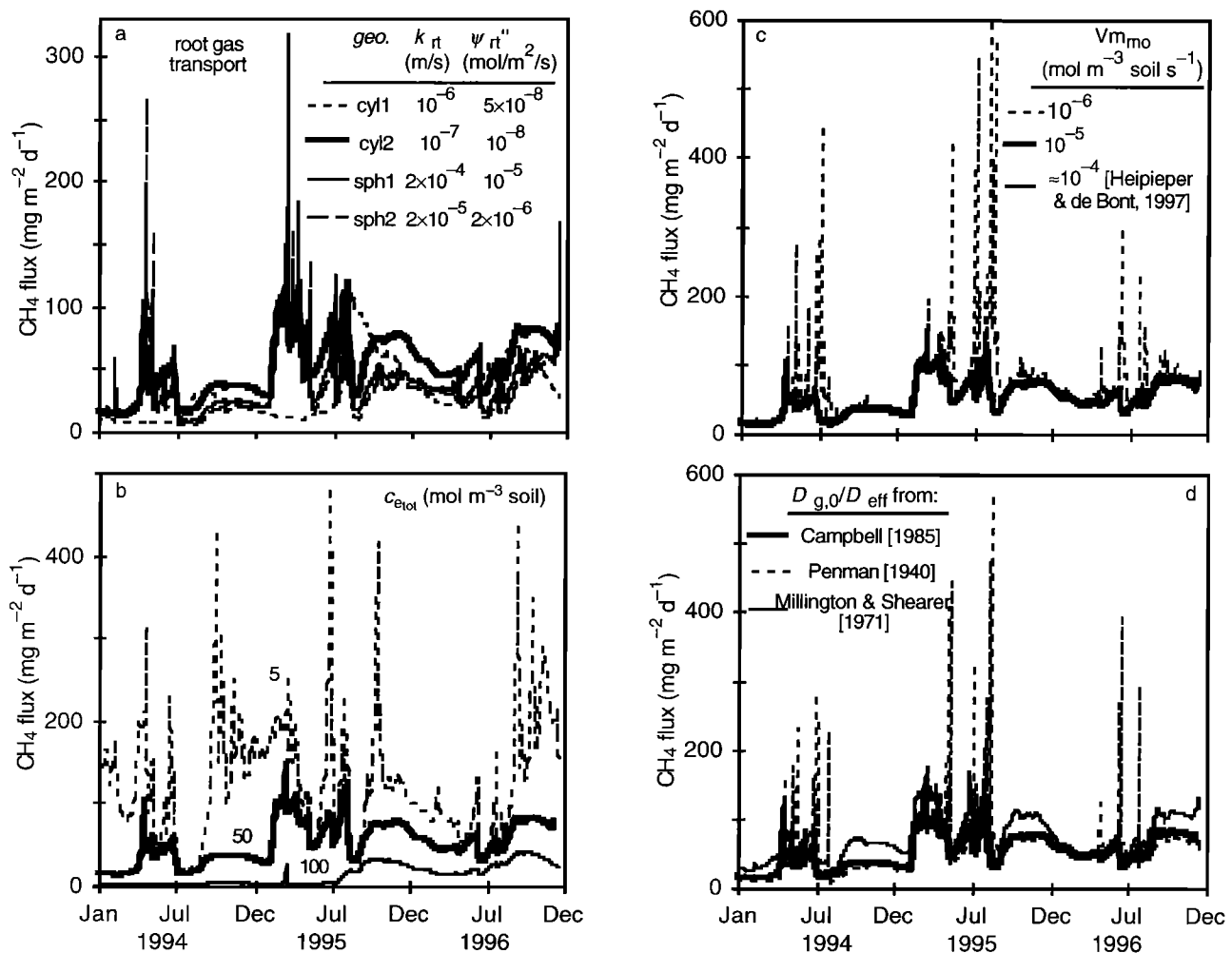
Figure 9. (a-g) Sensitivity analysis for modeled methane fluxes at Koole. The result of the default parameterization (Tables 3 and 4) (thick solid line) is plotted in each graph. Deviations from this default are indicated in the graphs. Note the differences in the yaxis.

given the large number of uncertainties this would not be very meaningful, as the model would get more descriptive than explanatory. Moreover, for a realistic comparison between model and experiment, one should also consider the large spatial variation in both measured fluxes and in site-specific sensitive parameters. Instead, we will have a closer look at the sensitivity analysis of the current model with the default parameterization, which will give insight in various interactions and the role of various processes.

3.5.1. Sensitivity analysis.

Most graphs (Figures 9) show emission patterns with an episodic character due to soil diffusive fluxes of methane upon a falling water table. This has been measured several times [Moore et al., 1990; Windsor et al., 1992; Shurpali et al., 1993]. However, peaks do not always occur when the water table is dropping. The simulations show that the most pronounced peaks occur if plant gas transport capacity is low (Figure 9a), if the electron acceptor pool is low (Figure 9b), if potential methane oxidation is low (Figure 9c), or if the effective diffusion coefficient is high (Figure 4 and 9d). These episodic patterns cannot be predicted, because of the large uncertainty in the determining parameters.

Electron acceptor cycling may interfere greatly with methanogenesis (Figure 9b). Reduction of electron acceptors

may typically take a week or month [Segers and Kengen, 1998], while the reoxidation of electron acceptors may be much faster (≈ 1 day [Segers and Leffelaar, this issue]). This explains why a short period of a low water table can have a long-lasting effect on methane fluxes [Freeman et al., 1994]. The exact nature of electron acceptors in peat soils is not well known [Segers and Kengen, 1998], which makes it impossible to estimate their concentrations from readily available information, such as peat type.

In their modeling study, Arah and Stephen [1998] concluded that increases in root gas transport capacity decreases methane emission, because of the increase of oxygen input in the soil. However, their simulations were performed for permanently saturated soil in steady state situation. Segers et al. [this issue] showed that the simulation time affects the sensitivity of methane emissions for root gas transport capacity. Figure 9a shows that for soils with a fluctuating water table the picture is even more complicated. At low transport capacities (sph1 and sph2) the emissions are generally low with large peaks when water table drops (Figure 5), due to large stocks of accumulated methane. At intermediate transport capacities (cyl2) the baseline emissions are higher. At high transport capacities (cyl1) the emissions are also low, because of the high oxygen input.
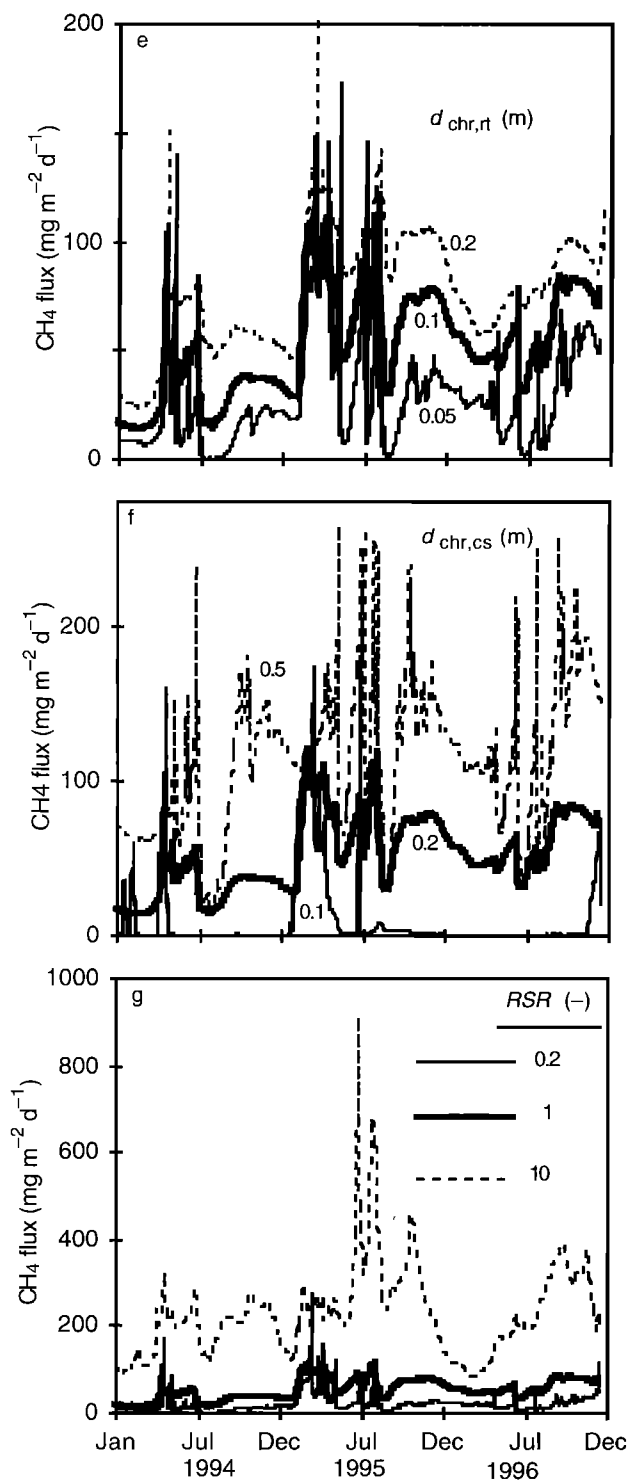
Figure 9. (Continued)

Changes in the distribution over depth of the roots and the stable soil carbon pool, greatly affect methane emissions (Figures 9e and 9f). This is due to the strong interactions with the water table. The depth dependence of the processes is illustrated in Figure 10 which shows that ignoring the depth dependence would result in a loss of mechanistic understanding.

The relation between the effective diffusion coefficient and the gas filled pore space is uncertain (Figure 4), and methane fluxes are sensitive to this relation (Figure 9d). The higher the effective diffusion coefficient, the lower the methane fluxes. This can be explained by the enhanced oxygen inflow, especially in peat soils with a high bulk density (as ours) resulting in a relatively large nearly water-saturated zone with diffusion-limited oxygen consumption.

At our sites, spatial variation in methane fluxes could be described by a correlation with sedge biomass but not with other nonmosses [*van den Pol-van Dasselaar et al.*, 1999b] Though the number of replicates was small, this indicates that the classification of the vegetation into mosses and nonmosses is probably too coarse to explain the effect of vegetation on methane fluxes [*Schimel*, 1995]. The sensitivity analysis shows that several plant-related factors may greatly influence methane fluxes. However, quantitative knowledge on relevant plant properties (such as root-shoot ratio, root turnover, root gas transport capacity, possibly root exudation) is lacking to make a process model more plant specific.

3.5.2. Mass flow. As discussed in section 2.1, mass flow (convection) may affect methane fluxes. The role of mass flow was investigated by comparing results of a simulation with mass flow to results of a simulation without mass flow (Figure 11a). In the model the peaks in methane emissions are enhanced by mass flow, whereas winter fluxes are reduced by mass flow, which can be explained by the effect of mass flow on electron acceptor concentrations. These are reduced in the top layer due to the evapotranspiration deficit but may be temporarily enhanced in deeper layers due to infiltration from oxic top layers (Figure 11b) These effects decrease with time (Figure 11a) due to leaching of the total pool of electron acceptors as a result of the precipitation surplus However, in translating this effect to the field, one has to be careful, firstly because we ignored adsorption of oxidized and reduced electron acceptors, and secondly, because we did not include the source of oxidized and reduced electron acceptors This source could be precipitation or soil carbon transformed into humic acids [*Lovley et al.*, 1996].

Mass flow also affects methane fluxes via the leaching of methane, which was 10% of emitted methane in the default situation (data not shown). The fate of this methane is unclear.
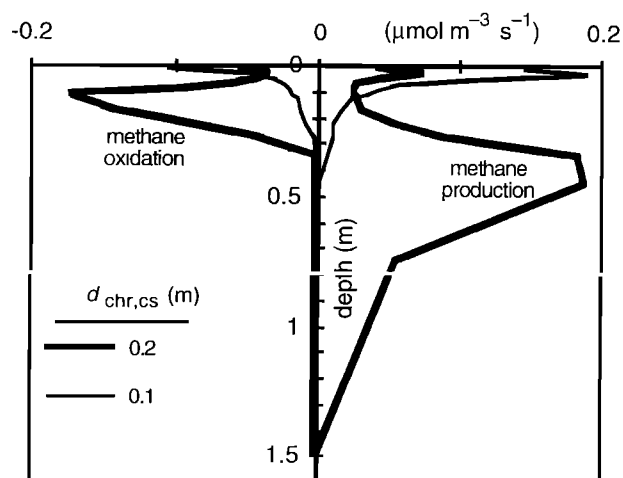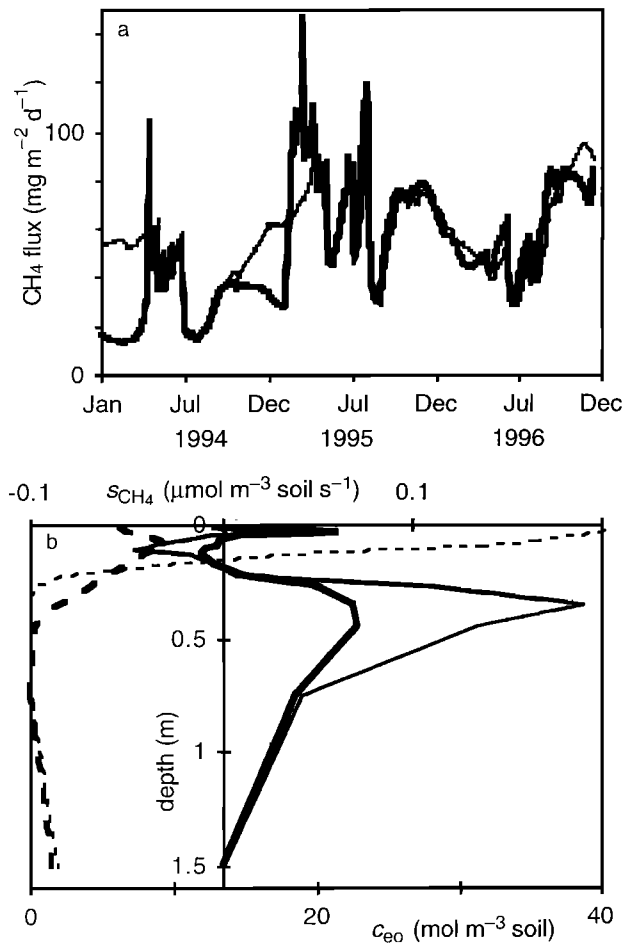

Figure 10. Time-averaged simulated methane production and methane oxidation as a function of depth at Koole from 1994 to 1996. Methane production is positive, methane oxidation is negative. Parameters are in Tables 3 and 4, except for $d_{chr,cs}$, which is indicated in the graph.

Figures 11. Simulations with (thick line) and without (thin line) mass flow at Koole. Parameters are in Tables 3 and 4. (a) Methane flux. (b) Net methane production, s_{CH_4} (solid lines), and (oxidized) electron acceptor concentrations, c_{eo} (dashed lines), both as function of depth, time averaged over the first 100 days of 1994

but it may partly show up in the ditches whose methane emission on a area basis is higher than the methane emissions from the land [van den Pol-van Dasselaar et al., 1999a].

3.6. Soil Methane Concentrations

Like methane fluxes, soil methane concentrations are the result of the balance between methane production, methane oxidation and methane transport. Hence, analyzing these concentrations is meaningful for understanding methane fluxes and testing the performance of a process model. Figure 12 shows that in the default situation, simulated soil methane concentrations are about 1 order of magnitude higher than measured soil methane concentrations. This could be due to an overestimation of simulated methane production, due to an underestimation of simulated root gas transport, or due to the not measured spatial variation in methane concentrations (as measurements were only at one spot). An underestimated potential methane oxidation is not likely, as the considered depth is mostly below the water table, as rhizospheric methane oxidation is limited by oxygen, and as enhanced methanotrophic oxygen consumption promotes methane production, because of increased anaerobiosis and decreased electron acceptor reoxidation [Segers and Leffelaar, this

issue]. Both in the experiment and in the simulation the seasonal trends of soil methane concentration at this depth reflect the variation in water table, with drops in concentration due to drops of the water table (Figure 5)

3.7. Comparison of Full Soil Layer Model With Simplified Soil Layer Model and Homogeneous Soil Layer Model

Three models were used to simulate methane dynamics at the soil layer scale [Segers et al., this issue]. The first model was the full soil layer model, in which the system is represented by a set of single-root model systems (equations (10)-(11)). The second model was the simplified soil layer model, in which the single-root model systems were aggregated into two fractions: oxygen saturated and oxygen unsaturated. The third model was the the homogeneous soil layer model in which a soil layer is considered homogeneous and the kinetic model is applied directly

The simplified and the full soil layer model result in similar methane fluxes, whereas the homogeneous soil layer model results in higher methane fluxes (Figure 13). The difference between the homogeneous soil layer model and the two other models is caused by differences in plant-mediated methane transport, which is enhanced in the homogeneous model by artificial mixing [Segers et al., this issue]. Aeration and net methane production are almost the same for the three models (data not shown), because in all cases, the aeration is mainly controlled by the water content profile. In the studied case (Koole), roots contribute little to aeration, because the zone with a high root density (top soil) is often aerated via the water-unsaturated soil matrix.

The differences in methane fluxes between the homogeneous and the full model are small relative to the differences in methane fluxes between various values for $d_{chi, es}$ and $d_{chi, it}$ (Figures 9e and 9f). Hence the considered heterogeneities at the profile scale seem to be more important than the considered heterogeneities within a soil layer. The strong influence of these profile scale parameters can be understood in terms of their influence on the electron balance, via the oxygen input. With low values of $d_{chi, es}$ and $d_{chr, rt}$ the oxygen sink in the surface layers increases, which leads to a higher oxygen input into the system, because in the surface layers oxygen uptake is often not limited by oxygen transport.
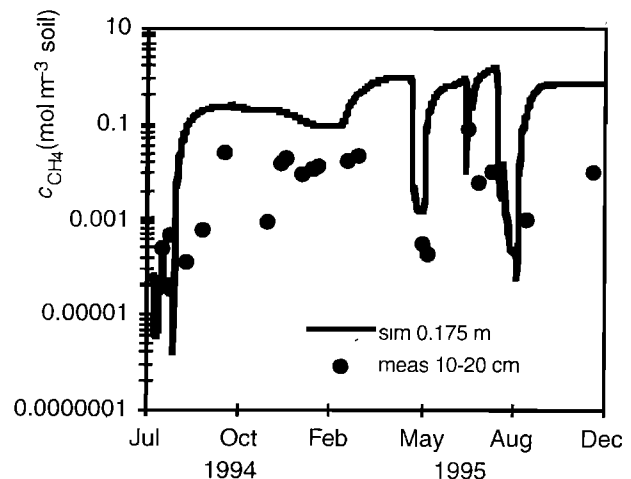

Figure 12. Simulated and measured [van den Pol-van Dasselaar et al., 1998] soil methane concentrations at Koole.
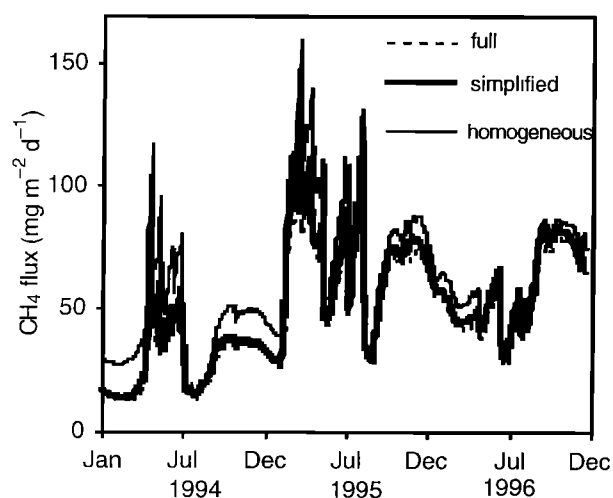
Figure 13. Effects of model structure at the soil layer level on simulated methane fluxes at the plot level at Koole. The models are derived by *Segers et al.* [this issue] and discussed in the text. Note that the difference between the lines of the full and simplified model is very small.

Moreover, fewer roots in deeper layers hamper methane export and increase methane oxidation (=oxygen input) when the water table drops.

4. Comparison With Other Models

Several other process models for wetland methane fluxes have been developed. We will discuss these other models in decreasing order of (spatial) detail.

4.1. Soil Layer Models

In soil layer models [*Walter et al.*, 1996; *Arah and Stephen*, 1998] the soil is divided in several layers to explicitly account for vertical gradients. Each soil layer is considered as homogeneous. The model of *Arah and Stephen* [1998] comes closest to our model, because they use oxygen, methane, and in an extension, electron acceptors as state variables, whereas *Walter et al.* [1996] use only methane as state variable. The omission of oxygen as a state variable seems attractive because methane oxidation can be estimated as a fraction of emitted methane, using the frequently applied technique of specifically inhibiting methanotrophs. However, reported oxidation fractions are highly variable [*Epp and Chanton*, 1993; *King*, 1996; *van der Nat and Middelburg*, 1998], and furthermore, there may be methodological problems due to effects of the inhibitor on other processes than methane oxidation, directly [*Frenzel and Bosse*, 1996, *Lombardi et al.*, 1997] or indirectly [*Segers and Leffelaar*, this issue].

Our sensitivity analysis shows that the parameterization of a methane flux model is crucial for the model results. *Arah and Stephen* [1998] used a detailed set of experiments on methane production, methane oxidation, and gas transport [*Nedwell and Watson*, 1995; *Stephen et al.*, 1998], and one fit parameter to parameterize their model and succeeded well in describing methane fluxes for a short period (10 days) from the investigated, permanently saturated, peat core. This success supports the soil layer approach. However it is still hard to transfer their model to other sites without the same amount of

measurements, because laboratory methane production and oxidation rates are very hard to relate to environmental variables [*Segers*, 1998]. By contrast, *Walter et al.* [1996] parameterized their model with a set of assumed parameters, in combination with two fit parameters and a measured time series of soil methane concentrations and methane fluxes. With this method they achieved a close correspondence between simulated and measured methane fluxes. However, they analyzed the sensitivity for only part of the assumed parameters, and not all parameter values can be traced in their paper, which makes it hard to compare their model with ours.

4.2. Ecosystem Models

In ecosystem models [*Cao et al.*, 1996; *Potter*, 1997; *Christensen et al.*, 1996] the soil is considered as a whole, and vertical gradients in the soil are ignored or implicitly accounted for. In all these models, methane production is connected somehow to net primary production (NPP), which enables extrapolation via NPP models.

From a process point of view one of the crucial factors in ecosystem models is the incorporation of the effect of the water table. Both *Cao et al.* [1996] and *Potter* [1997] multiply methane production with an empirical factor that decreases with lower water tables. Qualitatively, this is reasonable, but quantitatively, it is questionable whether a conservative relationship exists, because this relationship depends on the (depth distribution of) C-mineralization and the presence of electron acceptors. For parameterization of the relation between water table and methane production, data on the relation between water table and methane emission from the field [*Cao et al.*, 1996] or cores [*Potter*, 1997] were used. This is rather crude, because in these emission data also methane oxidation and transport are included. Furthermore, in both papers the large variation in the relation between water table and methane emission is ignored.

In all ecosystem models, methane is not present as a state variable, implicitly assuming a small delay between methane production and emission (less than the timescale of interpretation). As the timescale of root-mediated gas transport is typically larger than 1 day [*Stephen et al.*, 1998, *Liblik et al.*, 1997, *Segers et al.*, this issue], one has to be careful in interpreting these kind of models on a daily basis.

Christensen et al. [1996] ignored water table effects and assumed that methane flux was a fraction (3 ± 2%, based on literature) of aerobic respiration, the latter being almost similar to net primary production on an annual basis. So, on an annual basis, their model basically comes down to a proportional relation between methane flux and simulated net primary production. They also simulated monthly methane emissions, by assuming that they depend on temperature in the same way as aerobic respiration, but did not test this assumption, nor the simulated monthly methane fluxes. So given the present knowledge, the model of *Christensen et al.* [1996] may be suited for estimation of methane emission over large areas on an annual timescale but is not likely to represent the underlying processes.

5. Recommendations for Further Research

By scaling up from the kinetic scale to the plot scale we explicitly connected the knowledge at various scales to each other. Not surprisingly, during the procedure several uncertainties were revealed and several assumptions had to be made. Now, at the end the question arises: What are the most

important issues to be studied in the future? The answer to this question depends on the objective of the research. In the next three paragraphs we discuss three kinds of objectives.

For bottom-up (in contrast with top down (inverse atmospheric modeling [*Fung et al.*, 1991])) estimates of methane emissions over large areas, one needs predictive relations between methane fluxes and environmental variables that are easy to determine. The sensitive uncertainties in the plot scale model show that in the near future, process models will not be suited to determine these relations. However, the process models may help to find good descriptive models. For example, a time-averaged water table may be a better variable as an actual water table, because short-term water history also influences methane emissions via a release of methane after a fall of the water table and via a suppression of methane production by reoxidized electron acceptors after a rise of the water table.

However what would be the most effective way to bring the process knowledge to the plot scale? Daily methane emissions show large fluctuations that are very sensitive to several parameters and therefore probably also for plot-specific properties. To avoid part of these problems, it is worthwhile to look for a process model that operates at a large timescale, typically a year At this timescale the changes in stored methane and the cycling of electron acceptors (processes with a lot of uncertainties) are less important. What is important are the factors that determine the redox (electron) balance over the soil: the electron donor input (carbon mineralization and root exudation) and the electron acceptor input (oxygen). Aerobic respiration accounts for part of both the electron donor input and the electron acceptor input. This leaves as main electron donor input anaerobic carbon mineralization and root exudates not oxidized by oxygen. Then, the main electron acceptor input is oxygen used by methane oxidation and by electron acceptor reoxidation. This means that it is crucial to obtain more quantitative, depth-dependent, knowledge about root exudation and root turnover which, are potentially important sources of donors in the anaerobic zone. At the other side of the electron balance, oxygen input, first more knowledge should be obtained about the electron acceptors, leading to the questions. Are organic electron acceptors really important in peat? Do they capture a substantial amount of oxygen during reoxidation? Subsequently, a combination of experimental and theoretical research should determine the importance of the various ways of oxygen scavenging for methane oxidation and electron acceptor reoxidation (via the plant, at a stationary water table, events of falling water table).
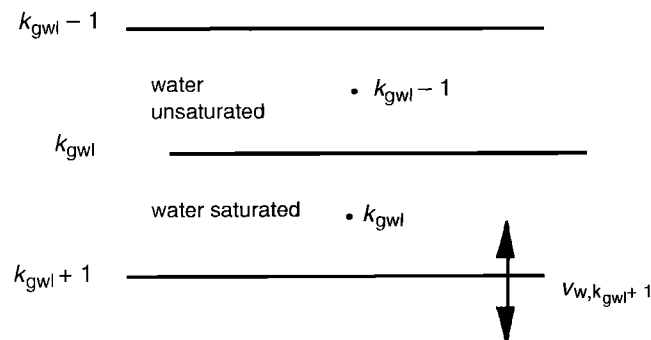

Figure A1. Illustration of spatial discretization around the water table for the water model; k is the index of the layer; v_w is the water flow.

To understand the seasonal dynamics in methane fluxes, one needs to know the seasonal dynamics of carbon supply (root exudation, root turnover) and plant gas transport capacity. Also, the possible temperature limitation of methanogens needs to be investigated. For understanding the peaks after a drawdown of the water table, accurate knowledge is needed on potential methane oxidation and the water and gas transport properties of the soil.

So, process models at larger timescales probably have less sensitive uncertain parameters than process models at short timescales. However, the models at larger timescales are harder to test against measured fluxes, because flux measurements are needed over a longer period with approximately the same time interval as for the process models at short timescales.

Appendix A. Discretization of Water Flow

Since the spatial discretization of the water flow is neither standard nor trivial, it is given below. State variables are the volumetric moisture contents in each discretized soil layer. At each time step, first the index of the groundwater level (k_{gwl}) is determined (Figure A1). A layer is considered saturated when the volumetric water content is within 0.001 of its maximum Hence occluded air is neglected for the water model. Then the soil water potentials in the soil layers above the groundwater level are determined as the sum of the gravity potential (which is set zero at the surface) and the matrix potential:

$$h_k = h_m(\theta_k) - z_k \quad \text{for } k = 1, ..., k_{gwl}. \quad (A1)$$

To obtain a continuous expression. the groundwater level is calculated from the equilibrium in the deepest unsaturated layer, with index $k_{gwl} - 1$:

$$gwlevl = h_{k_{gwl-1}}. \quad (A2)$$

Then, the flow from layer k_{gwl} to the next deeper layer is determined according to equation (15)·

$$v_w \, k_{gwl} + 1 = \frac{dtlevl - gwlevl}{R_{ditch}} \quad (A3)$$

Subsequently, the flows in the soil above the groundwater level are determined, which are constrained in case soil layer $k+1$ is saturated:

$$v_{w,k} = - k_k \frac{h_k - h_{k-1}}{\Delta z_k} \quad \text{for } k = k_{gwl}, ..., 1, \quad (A4a)$$

$$v_{w,k,max} = v_{w,k+1} - s_{w,k} \Delta z_k \quad \text{if layer } k \text{ is saturated.} \quad (A4b)$$

Note that equations (A4) require that the calculations start at the deepest soil layer. Finally, the flow below the water table is calculated in such a way that the water contents below the water table are constant:

$$v_{w,k} = v_{w,k-1} + s_{w,k-1} \Delta z_{k-1} \quad \text{for } k = k_{gwl}+1, ..., k_N. \quad (A5)$$

Appendix B: Incorporation of Profile Scale Transport Processes in the Single-Root Models

At the soil layer level it was assumed that gas exchange in water-saturated soil only occurs via the plants and via ebullition [*Segers et al.*, this issue] However. at the plot

scale also vertical diffusion and convection occurs. Especially just below the water table (penetrating oxygen) and in deep layers (with large distances between roots), this could be relevant. This vertical transport was incorporated in the model by adding an extra term, $sj_{i,k,m}$, to the rate equations for the concentrations (equation (11)) in each discretized soil layer k, for each component i, in each single-root model system m; $sj_{i,k,m}$ is equal to the discretized gradient of the flux density:

$$\overline{sj}_{i\,k,m} = \frac{\overline{J}_{i,k,m} - \overline{J}_{i,k+1\,m}}{\Delta z_k}.$$ (B1)

The length scale of the structures within a discretized soil layer (a few millimeter in densely rooted top soil, a few centimeter in deeper soil) is smaller than the discretized soil layer thicknesses (a few centimeter in the top and a few decimeter deeper in the profile). Consequently, a point near a root does not preferentially exchange gases or solutes with points near a root in the next upper or next deeper discretized soil layer. Therefore and because diffusion and convection are linear with concentrations, it is assumed that the flux densities only depend on the averages of the next upper and next deeper discretized soil layer:

$$\overline{J}_{i,k,m} = MAX(v_{w,k}, 0)\,\overline{c}_{aq,i,k-1} + MIN(v_{w,k}, 0)\,\overline{c}_{aq,i,k,m}$$

$$- D_{g\,eff,i,k}\frac{\overline{c}_{g,i,k,m} - \overline{c}_{g,i,k-1}}{\Delta z_{m,k}},$$ (B2a)

$$\overline{J}_{i,k+1\,m} = MAX(v_{aq,k+1}, 0)\,\overline{c}_{aq,i,k\,m} + MIN(v_{aq,k+1}, 0)\,\overline{c}_{aq,i,k+1}$$

$$- D_{g,eff,i,k+1}\frac{\overline{c}_{g,i,k+1} - \overline{c}_{g,i\,k\,m}}{\Delta z_{p,k}}.$$ (B2b)

The MAX and MIN functions are the result of the upwind discretization of convection [Patankar, 1980]. Using equations (B1) and (B2), the soil layer averaged component can be isolated by introducing an apparent mixing term:

$$\overline{sj}_{i\,k\,m} = \frac{\overline{J}_{i,k} - \overline{J}_{i\,k+1}}{\Delta z_k} + \xi_{mix\,sj,i,k}\,(\overline{c}_{i,k} - \overline{c}_{i,k,m}).$$ (B3)

Here the first term represents ordinary, soil layer averaged, profile scale transport, which is the same for all model systems m. The second term represents apparent mixing between the single-root model system within a discretized soil layer. From equations (B1) to (B3) mixing rate, $\xi_{mix,sj,i,k}$ can be expressed with

$$\xi_{mix,sj,i,k} = \frac{\alpha_{i,k}\,(- MIN(v_{aq,k},0) + MAX(v_{aq,k+1},0))}{(\varepsilon_{g,k} + \alpha_{i,k}\,\theta_k)\,\Delta z_k}$$

$$+ \frac{(\dfrac{D_{g,eff,i,k}}{\Delta z_{m,k}} + \dfrac{D_{g,eff,i,k+1}}{\Delta z_{p,k}})}{\Delta z_k\,(\varepsilon_{g,k} + \alpha_{i,k}\,\varepsilon_{w,k})}$$ (B4)

Here the first term represents upwind discretized convection, the second discretized diffusion. At the boundaries, $\xi_{mix,sj,i\,k}$ is calculated in a similar way resulting in slightly different expressions (not shown). The extra oxygen transport term reduces the oxygen sink for the roots, resulting in adaptation of the expressions for the dimensionless numbers β and κ [Segers and Leffelaar, this issue, equations (45) and (53)].

$$\beta = \frac{k_{it}\,(\alpha\,c_{g.atm.O_2} - \dfrac{\psi_{rt}''}{k_{rt}})}{(V_{ae}\,\omega\,s_{icm} - sj_{O_2})r_{rt}}.$$ (B5)

Cylinder

$$\kappa = \frac{2\,r_{rt}\,\varphi''_{O_2} + \overline{sj}_{O_2}}{V_{ae}\,s_{rcm}\,(R^2 - r_{it}^2)}.$$ (B6a)

Sphere

$$\kappa = \frac{3\,r_{rt}^2\varphi''_{O_2} + \overline{sj}_{O_2}}{V_{ae}\,s_{icm}\,(R^3 - r_{it}^3)}.$$ (B6b)

In this way the other equations of the simplified single-root model [Segers and Leffelaar, this issue] remain unchanged

Notation

a_1	regression coefficient for relation between surface temperature and radiation. K m^2 s J^{-1}.
a_2	regression coefficient for relation between surface temperature and radiation, K.
b	rate of change in soil gas concentration due to bubble release from a soil volume (by definition negative). mol m^{-3} soil s^{-1}
c	soil concentration of gas or solute. mol m^{-3} soil.
c_p	heat capacity. J K^{-1} m^{-3} soil.
C_{sh}	standing biomass of shoots. kg dw m^{-2} soil.
$C_{sh\,har}$	annually harvested biomass of shoots. kg dw m^{-2}.
c_{rt}	root density per soil volume. kg dw m^{-3} soil.
C_{it}	root density per soil area. kg dw m^{-2} soil.
$d_{ch\,it}$	characteristic root depth. m soil.
$d_{chr,cs}$	characteristic depth of stable soil carbon. m soil.
dtlevl	water level in ditches. m.
$D_{g,eff}$	effective gaseous diffusion coefficient. m^3 gas m^{-1} soil s^{-1}.
$D_{g,0}$	molecular gaseous diffusion coefficient. m^2 gas s^{-1}.
$f_{lab,it}$	fraction of decayed roots allocated to labile soil carbon.
$f_{lab,sh}$	fraction of decayed shoots allocated to labile soil carbon
f_C	carbon fraction of plants. kg C kg^{-1} dw.
f_{hyst}	hysteresis factor to prevent oscillation in model structure (equations (9)).
$f_{ms,hat}$	harvested fraction of mosses.
$f_{sh,har}$	harvested fraction of shoots.
$f_{stb}(z)$	distribution over depth of carbon allocated to stable soil carbon, m^{-1}.
gwlevl	groundwater level, m.
h	enthalpy per volume of soil, J m^{-3} or water potential. m.
h_m	matrix water potential. m.
h_w	enthalpy per volume of water, J m^{-3} H$_2$O.
J	flux density, mol m^{-2} s^{-1}.
k	hydraulic conductivity. m s^{-1}.
k_{rt}	effective root surface transport coefficient, m^3 H$_2$O m^{-2} soil s^{-1}.
k_s	saturated hydraulic conductivity, m s^{-1}.
k_N	total number of soil layers.
M_C	molecular weight of carbon, kg mol^{-1}.
pond$_{thi}$	threshold for runoff of ponded water, m.
q	rate of change due to vegetation-mediated gas transport, mol m^{-3} s^{-1}.

rad	global radiation. $J\ m^{-2}\ s^{-1}$.
r_{rt}	root radius. m.
R	half the distance to the next root. m.
RSR	root shoot ratio.
R_{ditch}	resistance for exchange of water between soil column and ditch. s.
s	net production of a compound. mol m^{-3} soil s^{-1}.
s_{aecm}	aerobic C-mineralization. mol C m^{-3} soil s^{-1}.
s_{acm}	anaerobic C-mineralization. mol C m^{-3} soil s^{-1}
s_{1cm}	reference C-mineralization. mol C m^{-3} soil s^{-1}.
s_w	rate of change of water content by water uptake by roots, $m^3\ H_2O\ m^{-3}$ soil s^{-1}.
s_f	rate of change in concentration of gases and solutes due to vertical convection. and diffusion, mol m^{-3} soil s^{-1}.
t	time, s.
T	temperature, K.
T_s	temperature at soil surface. K.
v_w	water flow. $m^3\ H_2O\ m^{-2}$ soil s^{-1}.
Vm_{mo}	methane oxidation under ample supply of O2 and CH4. mol $m^{-3}\ s^{-1}$.
w	weight function for half the distance to the next root. m^{-1}.
z	spatial coordinate depth. m.
z_{litu}	maximum depth of litter allocation. m.
α	solubility. m^3 gas $m^{-3}\ H_2O$.
β	ratio of time constants of O_2 sink in the soil modified for vertical oxygen transport by convection and diffusion and O_2 transport in the root.
Δz	thickness of a soil layer. m.
Δz_m	distance to the grid point in the next higher soil layer, m.
Δz_p	distance to the grid point in the next deeper soil layer, m.
ε_g	volumetric gas content (gas-filled pore space), m^3 gas m^{-3} soil.
$\varepsilon_{g,cr}$	volumetric gas content above which convection may occur, m^3 gas m^{-3} soil.
θ	volumetric moisture content, $m^3\ H_2O\ m^{-3}$ soil.
θ_s	saturated volumetric moisture content, $m^3\ H_2O\ m^{-3}$ soil.
κ	root O2 release relative to the O2 demand for aerobic respiration.
λ_h	thermal conductivity, $J\ m^{-1}\ K^{-1}\ s^{-1}$.
v_{ae}	stoichiometric constant for aerobic respiration.
$\xi_{mix,sf}$	apparent mixing coefficient due to vertical transport. s^{-1}.
ρ	bulk density, kg dw m^{-3} soil.
τ_{clab}	time constant of turnover of labile soil carbon, s.
τ_{cstb}	time constant of turnover of stable soil carbon, s.
τ_{rt}	time constant of root turnover. s.
τ_{sh}	time constant of shoot turnover, s.
φ''	flux density of gas through root surface, mol m^{-2} soil or root s^{-1}.
ψ_{rt}''	root respiration per gas-exchanging root area, mol $O_2\ m^{-2}$ active area s^{-1}.
ω	total oxygen sink relative to oxygen sink for aerobic respiration.

Compounds

eo	electron acceptor.
er	reduced electron acceptor.

c_{lab}	labile soil carbon.
c_{stb}	stable soil carbon.

Subscripts

aq	aqueous phase.
atm	atmosphere.
i	index of compound.
g	gas.
k	index of discretized soil layer.
k_c	index of deepest gas-continuous discretized soil layer.
k_{gwl}	index of discretized soil layer below the deepest water-unsaturated soil layer.
m	index of single-root model system.

Other symbols

$=$	averaged over single-root model system. averaged over soil layer.

References

Arah, J. R M . and K D Stephen. A model of the processes leading to methane emission from peatland. *Atmos Environ.. 32.* 3257-3264. 1998

Bartlett. K B . and R C Harris. Review and assessment of methane emissions from wetlands. *Chemosphere. 26.* 261-320. 1993

Bellisario. L M . J L Bubier. T. R Moore. and J P Chanton. Controls on CH₄ emissions from a northern peatland. *Global Biogeochem Cycles. 13.* 81-91. 1999

Belmans. C . J G Wesseling. and R A Feddes. Simulation model of the water balance of a cropped soil: SWATRE. *J Hydrol . 63.* 271-286. 1983.

Bernard. J. M . and K. Fiala. Distribution and standing crop of living and dead roots in three wetland *Carex* species. *Bull Torrey Botan Club. 113.* 1-5. 1986

Bernard. J M . D Solander. and J. Kvet. Production and nutrient dynamics in *Carex* wetlands. *Aquat Bot.. 30.* 125-147. 1988.

Boelter. D. H . Physical properties of peats as related to degree of decomposition. *Soil Sci Soc. Am Proc . 33.* 606-609. 1969

Brinson. M M . A E Lugo. and S Brown. Primary productivity decomposition and consumer activity in freshwater wetlands. *Annu Rev Ecol Syst . 12.* 123-161. 1981.

Brown. D A . Gas production from an ombotrophic bog – Effect of climate change on microbial ecology. *Clim Change. 40.* 277-284. 1998

Campbell. G. S.. *Soil Physics with Basic. Transport Models for Soil Plant Systems.* 150 pp . Elsevier Sci.. New York, 1985

Cao. M K . S Marshall. and K Gregson, Global carbon exchange and methane emissions from natural wetlands: Application of a process-based model. *J. Geophys Res.. 101.* 14,399-14,414. 1996.

Chapman, S J . and M. Thurlow. Peat respiration at low temperatures. *Soil Biol Biochem . 30.* 1013-1021. 1998.

Christensen. T R . I C. Prentice. J Kaplan. A Haxeltine. and S Sitch. Methane flux from northern wetlands and tundra - an ecosystem source modeling approach. *Tellus Ser. B. 48.* 652-661. 1996

Conrad. R.. Mechanisms controlling methane emission from wetland rice fields. in *Biogeochemistry of Global Change.* edited by R. S Oremland. pp. 317-335. Chapman and Hall. New York, 1993.

De Jong. R . and P Kabat. Modeling water balance and grass production. *Soil Sci. Soc. Am J . 54.* 1725-1732. 1990.

De Vries. D A.. Thermal properties of soils. in *Physics of Plant Environment.* edited by W R van Wijk. pp 210-235. North-Holland, New York. 1963

Drake. H L . N G Aumen . C Kuhner. C Wagner. A Griesshammer. and M Schmittroth. Anaerobic microflora of Everglades sediments

Effects of nutrients on population profiles and activities, *Appl Environ Microbiol*, *62*, 486-493, 1996

Dunfield, P F , E Topp, C. Archambault, and R Knowles, Effect of nitrogen fertilizers and moisture content on CH4 and N2O fluxes in a humisol: measurements in the field and intact soil cores, *Biogeochemistry*, *29*, 199-222, 1995

Epp, M E , and J P Chanton, Rhizospheric methane oxidation via the methyl fluoride inhibition technique, *J Geophys Res*, *98*, 18,413-18,422, 1993

Feddes, R A , P J Kowalik, and H. Zaradny, *Simulation of Field Water Use and Crop Yield*, 189 pp., PUDOC, Wageningen, Netherlands, 1978

Feddes, R A ,P. Kabat, P. J T van Bakel, J. J B Bronswijk, and J. Halbertsma, modeling soil water dynamics in the unsaturated zone – State of the art, *J Hydrol*, *100*, 69-111, 1988

Feddes, R A , P J Kowalik, and H Zaradny, *Simulation of Field Water Use and Crop Yield*, 189 pp, PUDOC, Wageningen, Netherlands, 1978

Freeman, C , J Hudson, M A Lock, B Reynolds, and C Swanson, A possible role of sulphate in the suppression of wetland methane fluxes following drought, *Soil Biol Biochem*, *26*, 1439-1442, 1994

Frolking, S , and P Crill, Climate controls on temporal variability of methane flux from a poor fen in southeastern New Hampshire Measurement and modeling, *Global Biogeochem Cycles*, *8*, 385-397, 1994

Fung, I , J John, J. Lerner, E Matthews, M. Prather, L. P Steele, and P J Fraser, Three-dimensional model synthesis of the global methane cycle, *J Geophys Res*, *96*, 13,034-13,065, 1991

Heipieper, H J , and J A M De Bont, Methane oxidation by Dutch grassland and peat soil microflora, *Chemosphere*, *35*, 3025-3037, 1997

Hillel, D , *Soil and Water, Physical Principles and Processes*, 288 pp , Academic, San Diego, Calif , 1971

Hirschfelder, J. O , C. F Curtiss, and R B Bird, *Molecular Theory of Gases and Liquids*, 1249 pp , John Wiley, New York, 1964

Jackson, R. B , J Canadell, J. R. Ehleringer, H A Mooney, O. E. Sala, and E D. Schulze, A global analysis of root distributions for terrestrial biomes. *Oecologia*, *108*, 389-411, 1996

Johnson, L C , and A W H Damman, Decay and its regulation in *Sphagnum* peatlands, *Adv Bryol*, *5*, 249-296 , 1993

King, G M , In situ analysis of methane oxidation associated with roots and rhizomes of a Bur Reed, *Sparganium eurycarpum*, in a Maine Wetland, *Appl Environ. Microbiol*, *62*, 4548-4555, 1996

Koorevaar, P., G. Menelik, and C Dirksen, *Elements of Soil Physics*, 230 pp , Elsevier Sci., New York, 1983

Leffelaar, P A., Dynamic simulation of multinary diffusion problems related to soil, *Soil Sci*, *143*, 79-91, 1987

Leffelaar, P A , Dynamics of partial anaerobiosis, denitrification, and water in a soil aggregate simulation, *Soil Sci*, *146*, 427-444, 1988

Leffelaar, P A , *On Systems Analysis and Simulation of Ecological Processes, with Examples in CSMP, TST and FORTRAN*, 318 pp , Kluwer Acad , Norwell, Mass , 1999

Liblik, L. K , T, R Moore. J L. Bubier, and S D. Robinson, Methane emissions from wetlands in the zone of discontinuous permafrost. Fort Simpson, Northwest Territories, Canada, *Global Biogeochem Cycles*, *11*, 485-494, 1997

Lombardi, J E., M A Epp, and J. P Chanton, Investigation of the methyl fluoride technique for determining rhizospheric methane oxidation, *Biogeochemistry*, *36*, 153-172, 1997.

Lovley, D. R., J D Coates, E. L. Blunt-Harris, E. J P. Phillips, and J C Woodward, Humic substances as electron acceptors for microbial respiration, *Nature*, *382*, 445-448, 1996.

Loxham, M , and W Burghardt, Saturated and unsaturated permeabilities of North German peats, in *Peat and Water*, edited by C H Fuchsman, pp 37-59, Elsevier Sci., New York, 1986.

Magnusson, T , Carbon dioxide and methane formation in forest mineral and peat soils during aerobic and anaerobic incubations, *Soil Biol Biochem*, *25*, 877-883, 1993.

Makkink, G F., Testing the penman formula by means of lysimeters, *Int. J Water Eng*, *11*, 277-288, 1957.

Metsävainio, K , Untersuchungen uber das Wurzelsystem der Moorpflanzen, *Ann. Bot Soc. Zool Fenn. Vanamo*, *1*, 1-419, 1931.

Miller, P C., R. Mangan, and J. Kummerow, Vertical distribution of organic mattter in eight vegetation types near Eagle Summit, Alaska, *Holarct Ecol*, *5*, 117-124, 1982.

Millington, R J., and R J Shearer, Diffusion in aggregated porous media, *Soil Sci*, *111*, 372-378, 1971.

Minkkinen, K , and J Laine, Effect of forest drainage on peat bulk density and carbon stores of Finnish mires, in *Northern Peatlands in Global Climatic Change*, edited by R Laiho, J Laine and H. Vasander, pp 236-241, Edita, Helsinki, 1996

Moore, T R , and N T Roulet, Methane flux- water table relations in northern wetlands, *Geophys Res Lett*, *20*, 587-590, 1993

Moore, T R , N T Roulet, and R Knowles, Spatial and temporal variations of methane flux from Subarctic/Northern boreal fens, *Global Biogeochem Cycles*, *4*, 29-46, 1990

Nedwell, D B , and A Watson, CH4 production, oxidation and emission in a UK ombotrophic peat bog- Influence of SO4 from acid rain, *Soil Biol Biochem*, *27*, 893-903, 1995

Nykanen, H., J Alm, J. Silvola, K. Tolonen, and P. J. Martikainen, Methane fluxes on boreal peatlands of different fertility and the effect of long-term experimental lowering of the water table on flux rates, *Global Biogeochem Cycles*, *12*, 53-69, 1998

Okruszko, H., and M. Szymanowski, Correlation between bulk density and water holding capacity of fen-peats, in *Proceedings of the 9th International Peat Congress*, vol 3, edited by D Frederikson, pp 106-115, IPS, Helsinki, 1992

Päivänen, J , Hydraulic conductivity and water retention in peat soils, *Acta For Fennic*, *129*, 1-70, 1973

Patankar, S V , *Numerical Heat Transfer and Fluid Flow*, pp. 197, Hemisphere, New York, 1980.

Penman, H L , Gas and vapor movements in soil, I, The diffusion of vapors through porous solids, *J. Agric Sci*, *30*, 437-461, 1940

Potter, C S , An ecosystem simulation model for methane production and emission from wetlands, *Global Biogeochem Cycles*, *11*, 495-506,

Prather, M., R. Derwent, D. Ehhalt, P Fraser, E Sanhueza, and X Zhou, Other trace gases and atmospheric chemistry, in *Climate Change 1994, Radiative Forcing of Climate Change and an Evaluation of the IPCC IS92 Emissions Scenarios*, edited by J. T Houghton, L G Meira Filho, J Bruce, H. Lee, B A Callander, E. Haites, and K. Maskell, pp. 73-126, Cambridge Univ Press, New York, 1995

Puranen, R. M. Makila, and H Saavuori, Electric conductivity and temperature variations within a raised bog in Finland- Implications for bog development, *Holocene*, *9*, 13-24, 1999

Rappoldt, C., The application of diffusion models to an aggregated soil, *Soil Sci*, *150*, 645-661, 1990.

Rappoldt, C Diffusion in aggregated soil, Ph D. thesis, Wageningen Agric Univ , Wageningen, Netherlands, 1992.

Richards, L. A , Capillary conduction of liquids through porous mediums, *Physics*, *1*, 318-333, 1931.

Romanowicz, E. A., D. A Siegel, and P H Glaser, Hydraulic reversals and episodic methane emissions during drought cycles. *Geology*, *21*, 231-234, 1993

Saarinen, T , Biomass and production of two vascular plants in a boreal mesotrophic fen, *Can J Bot.*, *74*, 934-938, 1996

Schimel, J P , Plant transport and methane production as controls on methane flux from arctic wet meadow tundra, *Biogeochemistry*, *28*, 183-200, 1995

Schouwenaars, J M , and J P M Vink, Hydrophysical properties of peat relicts in a former bog and perspectives for *Sphagnum* regrowth, *Int. Peat J.*, *4*, 15-28, 1992

Segers, R., Methane production and methane consumption- a review of processes underlying wetland methane fluxes. *Biogeochemistry*, *41*, 23-51, 1998

Segers, R , and S W M. Kengen, Methane production as function of anaerobic carbon mineralization: A process model, *Soil Biol Biochem*, *30*, 1107-1117, 1998

Segers, R , and P. A Leffelaar, Modeling methane fluxes in wetlands with gas-transporting plants, 1, Single root scale, *J Geophys Res*, this issue

Segers, R., C Rappoldt, and P. A Leffelaar. Modeling methane fluxes in wetlands with gas-transporting plants, 2, Soil layer scale, *J Geophys Res.*, this issue

Shannon, R D , and J R. White, The effects of spatial and temporal variations in acetate and sulfate on methane cycling in two Michigan peatlands. *Limnol Oceanogr*, *41*, 435-443, 1996

Shaver, G R , and F. S. Chapin III, Production Biomass relationships and element cycling in contrasting arctic vegetation types, *Ecol Monogr.*, *61*, 1-31, 1991

Shurpali, N J, S. B Vernma, R J Clement, and D P. Billesbach, Seasonal distribution of methane flux in a Minnesota peatland measured by eddy correlation, *J Geophys. Res.*, *98*, 20,649-20,655, 1993

Silins, U., and R L. Rothwell, Forest peatland drainage and subsidence
affect soil water retention and transport properties in an Alberta
peatland. *Soil Sci Soc. Am J*, *62*, 1048-1056, 1998.

Sjors, H, Phyto- and necromass above and below ground in a fen,
Holarct Ecol., *14*, 208-218, 1991.

Stephen, K D., J R M. Arah, W Daulat, and R S Clymo, Root-
mediated gas transport in peat determined by argon diffusion, *Soil
Biol Biochem*, *30*, 501-508, 1998.

Szumigalski, A R, and S E. Bayley, Decomposition along a bog to rich
fen gradient is central Alberta, Canada, *Can J Bot*, *74*, 573-581,
1996

ten Berge, H. F M, *Heat and Water Transfer in Bare Topsoil and the
Lower Atmosphere*. 207 pp, Pudoc. Wageningen, Netherlands,
1990

Thormann, M N, and S E Bayley, Decomposition along a moderate
rich fen marsh peatland gradient in boreal Alberta, Canada,
Wetlands, *17*, 123-137, 1997

van Bakel, P. J T, A systematic approach to improve the planning,
design and operation of surface water management systems, a case
study, *Rep 13*, Inst Cultuurtechn Waterh, Wageningen,
Netherlands, 1986

van den Pol - van Dasselaar, A, M L van Beusichem, and O. Oenema,
Methane emission from wet grasslands on peat soil in a nature
preserve. *Biogeochemistry*, *44*, 205-220, 1999a

van den Pol-van Dasselaar, A, M L van Beusichem, and O Oenema,
Determinants of spatial variability of methane emission from wet
grasslands on peat soil in a nature preserve. *Biogeochemistry*, *44*,
221-237, 1999b

van der Nat, F J W A, and J. J Middelburg, Seasonal variation in
methane oxidation by the rhizosphere of *Phragmites australis* and
Scirpus lacustris, *Aquat Bot*, *61*, 95-110, 1998

van Hulzen, H, R Segers, P W. M van Bodegom, and P A Leffelaar,
Explaining the temperature effect on methane production, *Soil Biol
Biochem*, *31*, 1919-1929, 1999

van Wirdum, G., *Vegetation and Hydrology of Floating Rich Fens*, 310
pp, Datawyse, Maastricht, Netherlands, 1991

Waddington, J. M, and N T. Roulet, Groundwater flow and dissolved
carbon movement in a boreal peatland, *J Hydrol*, *191*, 122-138,
1997

Wallen, B, Above and below ground dry mass of the three main
vascular plants on hummocks on a subarctic bog, *Oikos*, *46*, 51-56,
1986

Walter, B P, M Heimann, R D Shannon, and J R White, A process-
based model to derive methane emissions from natural wetlands,
Geophys Res Lett, *23*, 3731-3734, 1996

Wang, Z P, D Zeng, and W.H Patrick, Methane emissions from
natural wetlands, *Environ Monit. Assess.*, *42*, 143-161, 1996.

Wilhelm, E., R Battino, and R.J Wilcock, Low-pressure solubility of
gases in liquid water, *Chem Rev*, *77*, 219-262, 1977

Williams, R J, and R. L Crawford, Methane production in Minnesota
peatlands, *Appl Environ. Microbiol*, *47*, 1266-1271, 1984

Windsor, J, T R Moore, N T Roulet, Episodic fluxes of methane from
subarctic fens, *Can J Soil Sci.*, *72*, 441-452, 1992.

Wrubleski, D A., H R. Murkin, A. G. van der Valk, and J W. Nelson,
Decomposition of emergent macrophyte roots and rhizomes in a
northern prairie marsh, *Aquat Bot*, *58*, 121-134, 1997

P A Leffelaar, and R Segers, Group Plant Production Systems,
Laboratory of Theoretical Production Ecology, Wageningen University,
PO Box 430, 6700 AK Wageningen, Netherlands.
(peter.leffelaar@pp.dpw wau.nl, reinoud segers@pp.dpw wau nl)